CERN – EUROPEAN ORGANIZATION FOR NUCLEAR RESEARCH

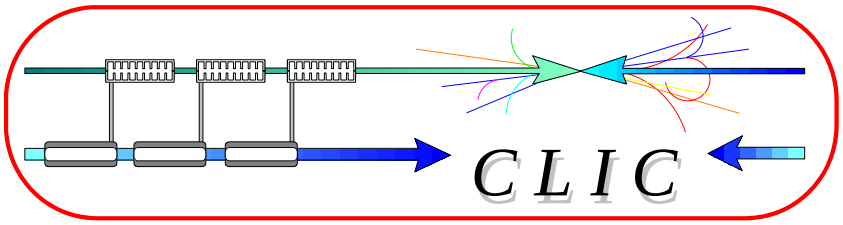

CLIC-Note-816

INVESTIGATION OF THE ENERGY DEPENDENCE OF BREAKDOWN PROPERTIES WITH A DC SPARK SETUP

Anita Hansen
Norvegian University of Science and Technology, Norway

Abstract

The Compact LInear Collider (CLIC) study is a site independent feasibility study aiming at the development of a realistic technology at an affordable cost for a future linear electron-positron collider. The European Organization for Nuclear Research (CERN) is one of the collaborators for the CLIC study. The CLIC Test Facility (CTF3) positioned at CERN provides testing of this technology, including the testing of the proposed radio-frequency (RF) structures in a two-beam concept to produce the necessary accelerating electric field as high as 100 MV/m to reach the goal of a nominal total energy of 3 TeV. One problem at such high accelerating fields is electrical discharges, i.e. sparks, damaging the inside of the RF structures as well as deflecting the trajectories of accelerated particles.

A Direct Current (DC) spark test setup is in use at CERN to aid the understanding of electrical discharges under vacuum conditions, also called vacuum arcs. In contrast to the more complex CTF3 setup, the DC spark setup is simple, fast and is solely devoted to study the discharge phenomenon, in-between two electrodes in ultra high vacuum.

For this thesis, several parameters governing a vacuum breakdown have been studied at different discharge energies, i.e. the energy that is available for a spark. The energy dependence of several parameters was examined for two RF structure candidate metals, copper and molybdenum, with discharges in the energy range 1 to 1000 mJ. The different parameters examined in this work are the size of the surface damage on the electrodes, the initial number of sparks needed to reach a stable, saturated field, and the saturated field.

The size of the surface damage was found to increase for increasing energy for both materials. At any energy, Cu reaches its saturated field within 2-8 sparks, while Mo need 30-50 sparks to achieve a saturated field. For Cu the saturated field decreases with increasing energy, contrary to Mo where the saturated field increases with increasing energy. Furthermore, the field enhancement factor and the corresponding local field have also been studied. The field enhancement factor is seen to increase with increasing energy and the local field is found to be constant for Cu. For Mo, the field enhancement factor is constant, while the local field is increasing with increasing energy. The lower limit of the discharge energy feasible with the present DC setup has been identified, as well as limitations of measuring the field enhancement factor on the cathode surface. In addition, another approach to explain the process of DC conditioning has been presented as well as a possible criterion to predict and thus avoid breakdowns.

Geneva, Switzerland
December, 2009

Master's thesis

Anita Hansen

Investigation of the energy dependence of breakdown properties with a DC spark setup

Trondheim December 2009

NTNU
Norwegian University of Science and Technology
Faculty of Natural Sciences and Technology
Department of Materials Science and Engineering

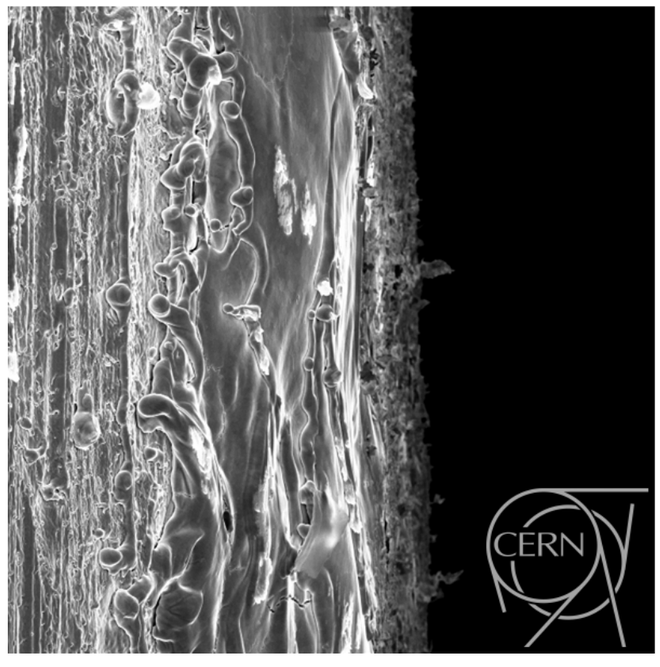

NTNU
Norwegian University of Science and Technology

NTNU
Norwegian University of Science and Technology

Master Thesis

Materials Technology

Investigation of the energy dependence of breakdown properties with a DC spark setup

Anita Hansen

December 2009

Norwegian University of Science and Technology
Faculty of Natural Sciences and Technology
Department of Materials Science and Engineering

European Organization for Nuclear Research
Technology Department
Vacuum, Surfaces and Coating Group

The front-page photo is a micrograph taken by A. Toerklep, at CERN. The image is from a DC spark molybdenum anode.

Abstract

The Compact LInear Collider (CLIC) study is a site independent feasibility study aiming at the development of a realistic technology at an affordable cost for a future linear electron–positron collider. The European Organization for Nuclear Research (CERN) is one of the collaborators for the CLIC study. The CLIC Test Facility (CTF3) positioned at CERN provides testing of this technology, including the testing of the proposed radio-frequency (RF) structures in a two-beam concept to produce the necessary accelerating electric field as high as 100 MV/m to reach the goal of a nominal total energy of 3 TeV. One problem at such high accelerating fields is electrical discharges, i.e. *sparks*, damaging the inside of the RF structures as well as deflecting the trajectories of accelerated particles.

A Direct Current (DC) spark test setup is in use at CERN to aid the understanding of electrical discharges under vacuum conditions, also called vacuum arcs. In contrast to the more complex CTF3 setup, the DC spark setup is simple, fast and is solely devoted to study the discharge phenomenon, in-between two electrodes in ultra high vacuum.

For this thesis, several parameters governing a vacuum breakdown have been studied at different discharge energies, i.e. the energy that is available for a spark. The energy dependence of several parameters was examined for two RF structure candidate metals, copper and molybdenum, with discharges in the energy range 1 to 1000 mJ. The different parameters examined in this work are the size of the surface damage on the electrodes, the initial number of sparks needed to reach a stable, saturated field, and the saturated field.

The size of the surface damage was found to increase for increasing energy for both materials. At any energy, Cu reaches its saturated field within 2–8 sparks, while Mo need 30–50 sparks to achieve a saturated field. For Cu the saturated field decreases with increasing energy, contrary to Mo where the saturated field increases with increasing energy. Furthermore, the field enhancement factor and the corresponding local field have also been studied. The field enhancement factor is seen to increase with increasing energy and the local field is found to be constant for Cu. For Mo, the field enhancement factor is constant, while the local field is increasing with increasing energy. The lower limit of the discharge energy feasible with the present DC setup has been identified, as well as limitations of measuring the field enhancement factor on the cathode surface. In addition, another approach to explain the process of DC conditioning has been presented as well as a possible criterion to predict and thus avoid breakdowns.

Acknowledgement

I would like to thank my academic supervisor Morten Kildemo at NTNU and my supervisor at CERN, Sergio Calatroni, for their professional guidance and support in my work, and for making it possible for me to write this master thesis at CERN. A very special thanks to my office mate and friend Helga Timkó, for motivation, guidance, and many fruitful discussions.

I would also like to thank Antoine Descoeurdes, Jan Kovermann, Holger Neupert and Wilhelmus Vollenberg for encouragement and assisting me in the lab. The professional insight of Mauro Taborelli and Walter Wuensch is greatly appreciated. Further, I am deeply grateful for the help from my colleague and friend Hugo P. Marques for troubleshooting and screwing flanges with me in the lab. The discussions and guidance in whiskers theory from Flyura Djurabekova and Kai Nordlund from the Helsinki Institute of Physics is greatly acknowledged.

Thanks to Anders Tørklep (for the front-page photo) and Patrick Alknes in the metallurgy section for taking SEM photos and other microscopic measurements of my samples. The help from Ivo Wevers with heat treatments and Delphine Letant-Delrieux with the XPS measurements is also acknowledged. Thanks to Luigi Leggiero for sample cutting, Leonel M. A. Ferreira for electropolishing and the chemistry laboratory for sample cleaning.

A big thank *you* and a great hug to my family and friends. And an extra smile to my fiancé Tor Arne, who's giving sense to it all: ☺

Anita Hansen
Geneva, December 2009

Contents

Abbreviations and Symbols

This section describes various acronyms, abbreviations, and symbols used throughout the text.

Abbreviations and acronyms

AFM	Atomic Force Microscope
bcc	body-centred cubic
BDR	BreakDown Rate
CERN	European Organization for Nuclear Research
CLIC	Compact LInear Collider
CT	Current Transformer
CTF	CLIC Test Facility
DC	Direct Current
EBSD	Electron BacksScatter Diffraction
fcc	face-centred cubic
FE	Field Emission
FN	Fowler–Nordheim
hcp	hexagonal close-packed
HV	High Voltage
KEK	High Energy Accelerator Research Organization
LEP	Large Electron–Positron [collider]
MD	Molecular Dynamics
NI	National Instruments
PIC	Particle-In-Cell
RF	Radio Frequency
SEM	Scanning Electron Microscope
SLAC	Stanford Linear Accelerator Center
SLC	Stanford Linear Collider
UHV	Ultra High Vacuum
XPS	X-ray Photoelectron Spectroscopy

Symbols

β	Field enhancement factor
β_{meas}	Measured field enhancement factor, not corrected values
C	Capacitance
d	Discharge gap
f_C	Correction factor for the voltage over the electrodes due to small capacitance difference
f_d	Correction factor for the gap being changed by breakdowns
f_p	Correction factor for β when the HV probe has been connected during FE measurements
E	Electric field
E_b	Breakdown field
E_{loc}	Local field also local breakdown field
$E_{b,meas}$	Measured breakdown field, not corrected values
E_{sat}	Saturated [breakdown] field
n	Number of sparks (on one spot)
R	Resistance
V	Voltage
V_0	Voltage from the power supply
V_d	Voltage seen by the electrodes
W	Electrostatic energy

1 Introduction

1.1 Background

CLIC project

The CLIC (Compact LInear Collider) project is a feasibility study for a future linear electron–positron collider operating in the TeV energy range. Until now, the highest centre-of-mass energy in electron–positron collisions — 209 GeV — was reached in the circular Large Electron–Positron (LEP) collider at CERN [1]. In the energy range to be explored, the electrons become ultrarelativistic because of their mass being so small comparable to their energy. The energy loss by synchrotron radiation in circular accelerators increases with the fourth power of the energy of the circulating beam, making a huge loss when going from GeV to TeV. It is therefore generally acknowledged that a *linear* accelerator is the only feasible and cost-effective way of building multi-TeV electron–positron colliders.

In order to make the linear accelerator as short as possible, the radio frequency (RF) accelerating structures need to achieve very high accelerating electric fields. The aim for CLIC is an accelerating field of 100 MV/m, corresponding to a surface field well above 200 MV/m [2, 3]. Conventional RF sources do not provide sufficient RF power for such high gradients, which is why CLIC relies upon a unique *two beam* concept. In this concept the main beam accelerates the particles, and the drive beam provide the necessary RF power for the accelerating structures in the main beam, see Fig. 1.1. The two beams lines act together like an energy transformer. [4]

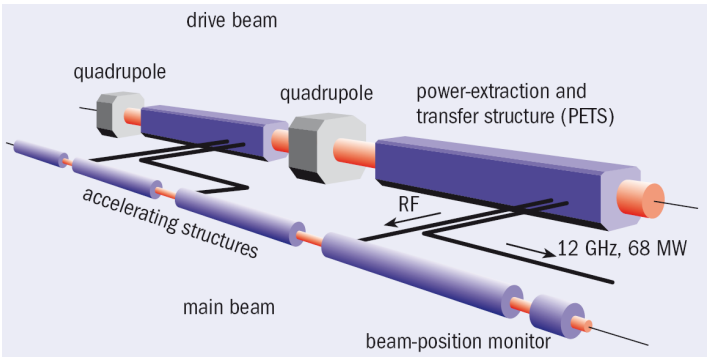

Figure 1.1: CLIC two-beam scheme, with the main beam accelerating the particles, powered by the lower-energy drive beam [1].

Background of breakdowns

An electrical breakdown is a discharge between two electrodes. The best known discharge phenomenon is lightning, in which the air between the electrodes (the clouds and the ground) is ionized. Electrical discharges occur in practical applications, ranging from the intentional in arc welding to the unintentional in fusion reactors and particle accelerators, and have been explored for the last 150 years.

An electrical breakdown in vacuum, which is discussed in this work, is usually of a smaller scale (here over μm distances) and is an even bigger mystery than gas discharges. Vacuum arcs have been studied for more than 50 years [5], and a complete understanding is still missing. The vacuum arc, just like a lightning, is a discharge between two electrodes, however, while lightning ionizes the medium in-between the two electrodes to make a plasma arc, it is not yet fully clear by what mechanism the arc plasma is created under high vacuum conditions, i.e. out of "nothing".

An important result from the vacuum breakdown experiments of Boyle, Kisliuk and Germer in 1955 [5] is: "It is found that field emission currents [...] flow before breakdown. These currents follow the Fowler-Nordheim equation[1] when field magnification due to surface irregularities on the cathode is taken into account." This is still a part of the present understanding of the breakdown process and is further discussed in Sec. 2.1.

Breakdown studies for CLIC

The accelerating field in CLIC is limited by two main effects: RF breakdown and fatigue cracking due to pulsed surface heating. (The latter phenomenon will not be further discussed in this work.) It has been found that breakdowns are beneficial in an initial stage, before having a beam in the RF accelerating structures. In the initial phase a high number of breakdowns occurs, creating a structure that is more stable with respect to the probability of having breakdowns at a later stage. This process (the initial phase) is called *conditioning*. However, breakdowns in RF structures cause surface damage, and later on breakdowns will cause beam instability, which in the worst case may cause loss of the beam at the collision point. Due to practical limitations during the operation of RF structures, the following must be taken into account: sufficiently fast RF conditioning, acceptable surface modification (from both the conditioning process and the accumulated breakdowns during the lifetime of the accelerator), and a sufficiently low vacuum level inside the structure during the RF pulse. [2]

The best accelerating structure produced for CLIC so far is made of copper. It was designed by CERN, manufactured by the High Energy Accelerator Research Organization (KEK) and assembled and tested at the Stanford Linear Accelerator Center (SLAC). It endured fields higher than 100 MV/m at nominal pulse length (i.e. 240 ns), with — as required — an extremely low probability of RF breakdowns. [3, 6]

Although the structure mentioned above fulfils the design requirements for high accelerating field combined with a low breakdown rate, and may be used for the feasibility demonstration of CLIC in 2010, optimization work for an even better structure continues. Every reduction

[1] see Eq. 2.1 in Sec. 2.1.

of necessary input power for the accelerating cavities would give a remarkable economic gain with respect to power consumption.

To complement the study of the effect of breakdowns which limit the operation of RF structures, a Direct Current (DC) spark system has been built at CERN. The DC setup is far simpler than the RF structure setup, allowing vacuum breakdowns to be studied in a highly controllable and less time consuming manner. The purpose of the DC setup is divided between (i) getting a better understanding of the breakdown phenomenon itself and (ii) as a test facility for RF structure candidate materials and surface treatments.

1.2 Motivation for this work

This work aims to get a better understanding of breakdowns and their parameters, with special emphasis on how the different parameters depend on the energy available for the electrical discharge. The main parameters are the conditioning speed, the saturated breakdown field, the local field, the field enhancement factor, and the surface damage on the cathode, as defined in Sec. 2.1–2.2. Another parameter is the breakdown rate, from which earlier experiments will be discussed (cf. Sec. 2.3), but the breakdown rate will not be investigated in this work.

The purpose of exploring the energy dependence by going to lower energies in DC is twofold:

(i) The energy available is suspected to influence the conditioning efficiency. Two of the possible outcomes of are that either when lower energy is available for each breakdown, even more breakdowns are necessary to condition the surface, or it could be that the highest energies cause too much surface damage, meaning that at lower energies it could be possible to obtain even higher fields with the same probability of breakdowns. Details on how this is measured is given in Sec. 3.1.

(ii) The exact amount of energy consumed by the breakdown in RF structures was for a long time not known. The energy available in the DC setup ($\sim$1 J) was designed to match the RF pulse energy of about 0.8 J [2]. However, it has recently been pointed out that only 7–36 % of the input pulse energy is dissipated through a breakdown [8].

The long conditioning phase seen for Mo in the DC setup, makes it a good material to study for the energy effect on the conditioning phase. Cu has shown a very short conditioning phase in the DC setup, while in RF cavities Cu has shown a quite long conditioning phase. Although the comparison between the DC setup and the RF cavities is not straightforward, especially regarding the conditioning process, it could be expected that by lowering the energy, conditioning could be seen for Cu in the DC setup as well as in RF. This difference between the DC and the RF setup could be attributed to the fact that in DC a much smaller area is being sparked repeatedly compared to the large area in the RF cavities and/or to the energy being lower in RF.

[2] Measured in RF structures at CTF2 (CLIC test facility 2) [7]

2 Theory

2.1 The electrical vacuum breakdown and its parameters

In the current understanding of the onset of a breakdown, a necessary criterion for ignition is the emission of electrons induced by an externally applied field [9]. These field emission (FE) currents are magnified by an enhanced surface field due to protrusions of nm size, also called field emitter, on the cathode surface. This is the origin of the enhanced local field (E_{loc}) at the surface, which is proportional to the externally applied field $E_{loc} = \beta E_{ext}$, β being the so-called field enhancement factor. The enhancement effect from the strongest field emitter could be related to its height, radius and sharpness [9].

Combined thermal and field evaporation of neutrals (and possibly ions) results in the appearance of atoms in vacuum. It is still not fully clear by which mechanism a — for breakdown — sufficient amount of atoms is evaporated, however, field evaporation theory [10, 11] in combination with thermal evaporation suggests that evaporation occurs mostly from the field emitters, that enhance the electric field and are heated up by the field emission current. Ionization of the evaporated atoms occurs through collision with electrons that are accelerated towards the anode. The positively charged ions will then bombard the cathode surface. When the neutral density reaches a certain threshold, an arc plasma will be formed between the electrodes [12], causing an electrical discharge. This is the process called *breakdown* or *sparking*. In the DC system utilized to study breakdown properties, the breakdown is directly related to discharging a capacitor, which will be further discussed in Sec. 2.4.

The field enhancement factor, β, is defined by $E_{loc} = \beta E_{ext}$ as mentioned above, and determined by the general Fowler–Nordheim (FN) equation [13, 14, 15]:

$$j_{FE}(E) = a_{FN} \frac{(eE_{loc})^2}{\phi t(y)^2} \exp\left(-b_{FN} \frac{\phi^{3/2} v(y)}{eE_{loc}}\right), \tag{2.1}$$

where j_{FE} is the electron field emission current density, ϕ is the work function, e the elementary charge, and $t(y)$ and $v(y)$ are elliptical integral functions. The constants a_{FN} and b_{FN} are:

$$\begin{aligned} a_{FN} &= \frac{e}{16\pi^2\hbar} = 1.5414 \cdot 10^{-6} \frac{\mathrm{A}}{\mathrm{eV}} \\ b_{FN} &= \frac{4\sqrt{2m_e}}{3\hbar} = 6.8309 \cdot 10^{9} \frac{1}{\sqrt{\mathrm{eV}}\mathrm{m}} \end{aligned} \tag{2.2}$$

when $[j_{FN}] = \mathrm{A/m^2}$, $[E_{loc}] = \mathrm{GV/m}$ and $[\phi] = \mathrm{eV}$, and where $\hbar$ is the reduced Planck constant, and m_e the electron mass in eV.

Experimentally, β can be determined by a series of field emission measurements, where the external field vs. the electron field emission current ($I = j_{FN} * A_e$) is measured. Substituting for the known constants and using for the elliptical integral functions the Wang–Loew approximation [16], the FN equation can be written into the form (2.3). This equation from is valid when temperature corrections and space charge limitations to field emission currents are neglected [7].

$$I = A_e \frac{1.54 \cdot 10^6 (\beta E)^2}{\phi} \exp\left(10.41\phi^{-1/2}\right) \exp\left(\frac{-(6.53 \cdot 10^3 \phi^{3/2})}{\beta E}\right) = \xi E^2 \exp\left(\frac{-\gamma}{E}\right) \quad (2.3)$$

where $[I] = \mathrm{A}$, $[E] = \mathrm{MV/m}$, A_e is the field emission area in m^2, $[\phi] = \mathrm{eV}$, and the constants γ and ξ are material and geometrical dependent parameters. For this work, the value $\phi = 4.5$ eV is used as an average for both polycrystalline Cu and Mo [17]. In a logarithmic presentation this gives:

$$ln\left(\frac{I}{E^2}\right) = ln(\xi) - \left(\frac{\gamma}{E}\right) \quad (2.4)$$

In Eq. 2.4 γ is the slope of a straight line, determined by a least-squares fit, which solved with respect to the dimensionless β gives:

$$\beta = \frac{6530\phi^{3/2}}{\gamma} \approx \frac{62335}{\gamma} \quad (2.5)$$

2.2 Nomenclature

The breakdown field E_b is simply defined by the highest voltage V the electrodes can sustain before breakdown occurs over the gap distance d;

$$E_b = \frac{V}{d} \quad (2.6)$$

For all the consecutive sparks (usually at least 100) completed at the same area (i.e. a spot), the results are summarized in a so-called *conditioning curve*, where breakdown field is plotted as a function of number of breakdowns.

When measuring the breakdown field of a material repeatedly on the same spot, the material may exhibit a conditioning phase, meaning that the field measured in the beginning increases (conditioning) or decreases (deconditioning) until a stable, saturated field is reached. The saturated breakdown field, E_{sat}, is defined as the average breakdown field after the conditioning phase[1].

2.3 DC spark experiments at CERN

The first of two DC spark setups (Fig. 2.1) has been in use at CERN since 2004 to study breakdowns and their properties, and the setup is explained in more detail in Sec. 3.1. Earlier experiments with the DC spark setup have revealed several important differences between

[1] In the case of no conditioning phase, E_{sat} is simply the average breakdown field.

materials and provided a better understanding of the breakdown phenomenon. Some of the most intriguing and important results will be discussed in this section.

Several methods have been used in conjunction with the DC spark setup are optical spectroscopy, Atomic Force Microscope (AFM) imaging of breakdown craters, SEM orientation mapping (by Electron BackScatter Diffraction (EBSD) method) surrounding the craters and chemical analysis of the specimen and crater surface after testing. These methods will not be further discussed here.

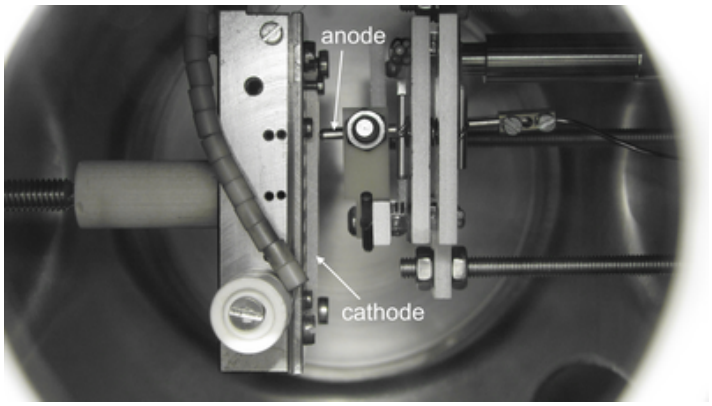

Figure 2.1: Vacuum chamber for DC breakdown testing. The electrodes are indicated.

Surface damage

Studies of material degradation by multiple sparks on one spot showed that the highest degree of erosion is always on the cathode surface, not the anode. Furthermore, among the three materials Cu, Mo and W, W can sustain the highest breakdown field and is the least susceptible to erosion, while Cu sustains the lowest field and has the highest material degradation [7]. Molecular dynamics (MD) simulations by H. Timkó et al. gave similar results regarding ranking the degree of erosion for Cu and Mo [18].

Conditioning

Mo is observed to have a rather long conditioning phase, which is explained by the very strong oxide layer that is naturally present on the surface. Mo with a thinner oxide layer has also been tested and it was then found that the conditioning phase shortens (down to 10 sparks with the thinnest layer). [19]

Cu, which has no significant natural oxide layer, is seen to reach the saturated field immediately, or after 1–2 sparks only. Artificially oxidized Cu gave a high breakdown field in the beginning (with a thick oxide layer for as long as 20 sparks) and then the breakdown field drops, meaning that Cu *de*conditions. [20]

Since Mo conditions and Cu deconditions, it has been suggested that the oxide layer of Mo is much weaker (in terms of breakdown resistance) than the bulk Mo, and the other way around for Cu; the Cu surface or oxide layer is stronger than the bulk Cu [21]. It has meanwhile been suggested that it is not the thickness of the oxide layer that determines the length of

the conditioning phase, but rather the stability of the oxide layer [22]. This topic, however, is outside the scope of the current work.

Breakdown rate measurements

Extensive studies of Cu regarding the breakdown probability and field enhancement factor development in breakdown rate mode have been performed at CERN by Descoeudres et al. [23]. As seen in Fig. 2.2(a), the working electric field is 200 MV/m and when the field drops to zero, a breakdown occurs. At this field, β increases until breakdown occurs after about 50 attempts. Then β decreases and stabilizes for the next 1000 attempts without any more breakdowns. When the working field is increased to 225 MV/m, see Fig. 2.2(b), again β is seen to grow until the first couple of breakdowns, after which the process is repeated: β continues to increase until another bunch of breakdowns occur.

The authors Descoeudres et al. concluded that there is a material dependent upper limit for the local field, βE that can be sustained: for the constant field, breakdown would occur whenever β has grown to achieve this upper limit. From the work of Descoeudres et al. it is also worth noting, that the local field was the only parameter that remained constant also when changing the spacing between the electrodes.

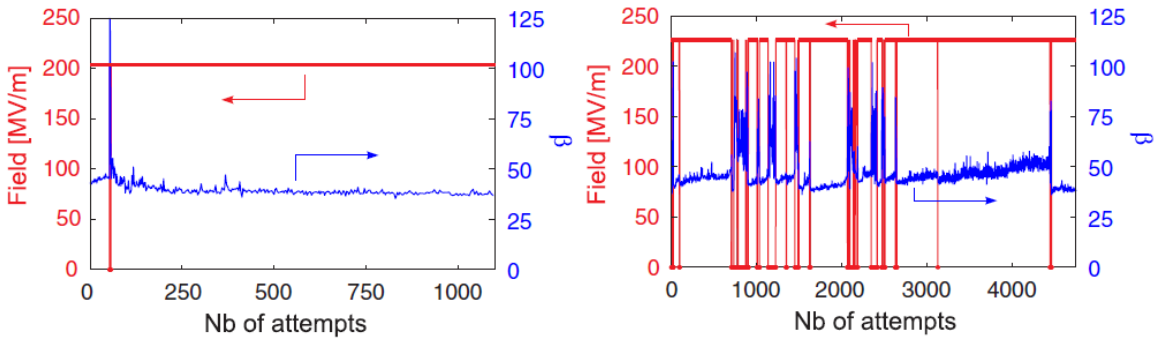

(a) 200 MV/m (b) 225 MV/m

Figure 2.2: Breakdown rate measurements with β for Cu at two different working fields. Breakdowns have occurred where the field drops to zero. In (a) β is seen to grow slightly before the first cluster of breakdowns at about 50 attempts, after which β decreases and stabilizes at ≈ 40. In (b) a higher field is applied, and β grows for each breakdown free period, up to roughly 50, resulting in a local field of ≈ 11 GV/m. [23]

Whisker growth

One possible mechanism that can explain β growth when only applying a high field, is a phenomenon called *whisker growth*. This was pointed out by Djurabekova et al. [24]. Whiskers are metallic filaments, they are highly conductive, and short circuit electrical components by bridging gaps between closely spaced electrical conductors. Whiskers have been a familiar issue in electrical components (especially of tin (Sn)) since the 1950s, and observations has shown that their growth is enhanced in the presence of electric fields ([25] and the references therein).

There is still a dispute on how whiskers erupt and grow from a metal surface, however, Djurabekova et al. [26] were able to simulate, by atomistic modelling, the first pico seconds of dislocation movements forming structures on the surface of pure Cu metal. These structures are believed to be the very beginning of whisker formation. Since the whiskers can be of µm thicknesses and up to mm lengths, if whiskers are at some point present on the DC samples it is not unlikely that they contribute to an increasing field enhancement factor, as shown in Fig. 2.2.

Material rankning

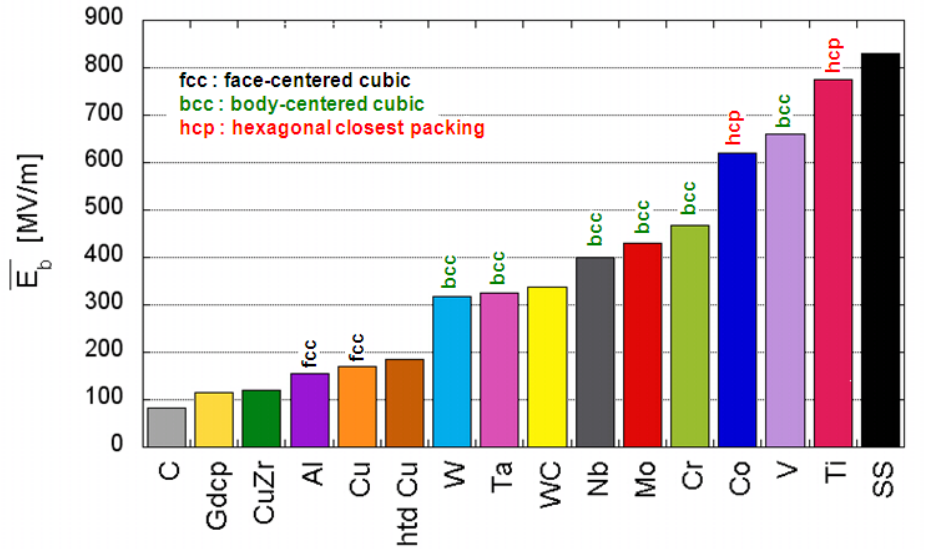

Figure 2.3: Ranking of materials in terms of the breakdown field reached after conditioning [27]. For pure metals it was suggested by Djurabekova et al. [24] that this was related to the crystal structure (as indicated) and dislocation movements. The crystal lattices are face-centred cubic (fcc), body-centred cubic (bcc) and hexagonal close-packed (hcp).

Meanwhile several materials have been tested, and a ranking from the lowest to the highest sustainable saturated breakdown field is given in Fig. 2.3. Material properties like the work function, melting point, electrical conductivity, etc. could not alone explain the ranking of the materials [27]. For the pure metals, the ranking seems to correlate with the crystal structure — fcc having the lowest breakdown field, then bcc, and finally the hcp structure having the highest. One can argue that the triggering of breakdown, and hence the field, is directly related to dislocation movements [24, 26], which are most energetic favourable in fcc, then bcc and finally hcp crystal structures [28].

2.4 Energy dependence

As circuit components, arcs have characteristics with negative resistance. Negative resistance means that the arc current is growing with dropping potential. The impedance of the arc will adjust to the total impedance of the circuit in order to short circuit it — this matter is further elaborated in [29]. This would mean that in the ideal case of a perfect short circuit

the energy stored in the discharging capacitor, W_C, will be consumed as ohmic losses with half of the energy over the circuit and half over the discharging electrodes. Where there is not a perfect matching, less energy goes to the discharge.

$$W = \frac{1}{2}W_C = \frac{1}{4}CV^2 \tag{2.7}$$

where W is the energy available for the discharge, C is the capacitance and V is the voltage applied over the electrodes.

When sparking repeatedly to measure conditioning, the voltage is not fixed, so the energy changes even with a given C (cf. Sec. 3.1). The applied voltage can range from 2 to 10 kV, which corresponds to the energy range 50 to 1500 mJ for $C = 27.5$ nF. This voltage range is taken into account when the energy is changed in the setup. Changing the energy available for a breakdown is hereinafter equivalent to changing the capacitance of the system.

3 Experimental

3.1 Measurement methods and technical details

The DC spark system has two main measurement modes: *Field Emission (FE) mode* for β measurements and *breakdown mode* for spark testing. Futhermore, we distinguish between breakdowns in *breakdown rate mode* and *spark cycle mode*. In the former, the same voltage is applied at each attempt, and the breakdown rate is then defined as the number of breakdowns out of the possible attempts. In the latter, also referred to as *conditioning mode*, the voltage is increased at each attempt (ramp-up) until breakdown, giving one complete cycle or scan, which is then repeated for the desired number of cycles. Each cycle correspond to one spark, and the breakdown field is usually presented as a function of number of sparks, giving a conditioning curve.

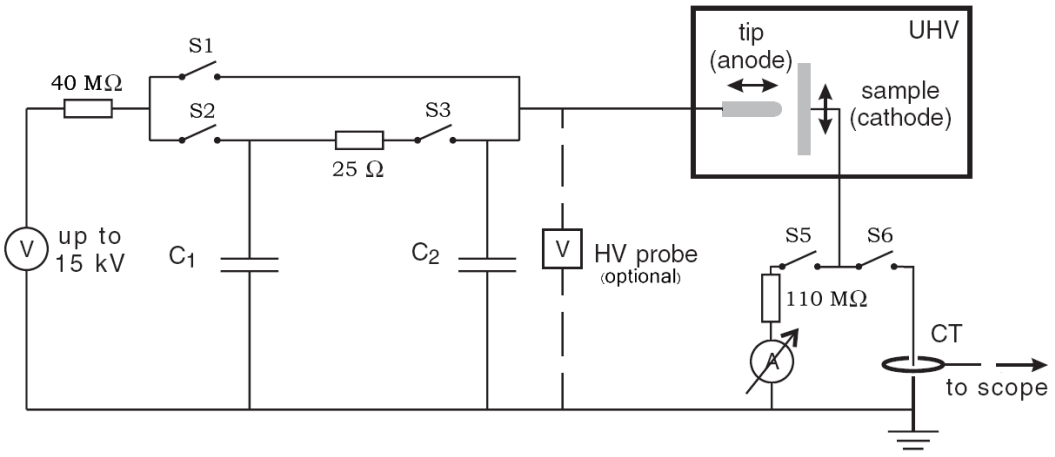

Figure 3.1: Schematic drawing of the DC spark system II, with the high voltage (HV) electronics and the ultra high vacuum (UHV) chamber having a pressure of $< 10^{-9}$ mbar. The energy available for breakdown is determined by the energy stored on the capacitor C_1. The purpose of C_2 is to limit overshoot voltages to the electrodes. In *field emission mode* switches S1 and S5 are closed, while in *breakdown mode* alternatingly switch S2, then S3 and S6 are being closed.

For this work the DC spark system II was used. The schematics of the experimental setup is shown in Fig. 3.1. The system was built in 2008, and has some more automated functions than the first, which is explained in full detail by M. Kildemo in [30]. System II has a stage that can move in 3 dimensions, and the change from FE mode to breakdown measurements are automatically performed by switches controlled by a National Instruments LabVIEW program

written for this purpose. It is also possible to change the capacitors C_1 and C_2 (Fig. 3.1), the ranges used in this system are shown in Tab. 3.1.

Table 3.1: Capacitances available for the DC system II. The values used to be 27.5 nF and 0.333 nF for C_1 and C_2 by default, respectively.

Capacitor	Capacitance [nF]
C_1	$27.5, 15, 2, 0.56, 0.1, 0.01$
C_2	$0.333, 0.167, 0.004$

Breakdown is registered if a current — exceeding a given threshold — is flowing through the current transformer (CT) coil. To assure correct detection of breakdown events, this is cross-checked with whether a vacuum pressure increase occurred.

Previously, the remaining charge on C_1 was measured. If no charge remained, a breakdown had occurred, whereas if some charge was left, information about the FE current could be obtained. This method is no longer applied, meaning we can no longer have quantitative information about FE *during* a spark scan when breakdown does not occur. However, in the present setup, a complete FE scan is usually performed before and after each spark scan, determining the field enhancement factor, β. FE current is measured by an ammeter directly in the circuit, during FE scans, switches S1 and S5 are closed.

3.1.1 Differences between the two breakdown modes

In-between each attempt in *breakdown rate mode* and between each spark scan in *spark cycle mode*, the field enhancement factor β is measured, allowing the determination of the local field $E_{loc} = \beta E$ for each breakdown. A notable difference between the two modes, is that in *breakdown rate mode* β is measured after each attempt, also when we do not have breakdown, while in *spark cycle mode* β is only measured before and after the cycle with the voltage ramp-up, and not in-between each attempt during the ramp-up. This will be further discussed in Sec. 5.2.

In *spark cycle mode*, see Fig. 3.1, switch S2 is first closed to charge C_1 from the voltage supply. The switch is then opened again while the switches S3 and S6 are closed for about 1 s, waiting for a breakdown. If no breakdown occurs then switches S3 and S6 are opened again, the voltage is increased and the process is repeated. Whereas in *breakdown rate mode* the voltage is constant, so the switches S2 and S6 remain closed during the whole procedure, and each attempt is separated only by opening and closing the switch S3 to recharge C_1. This means that in *breakdown rate mode*, the power supply is *always* connected to C_1, and after a breakdown, the power supply remains connected and will continuously feed energy to the electrodes.

Leaving the power supply connected to the electrodes is assumed to have no significant influence on the breakdown rate measurements. However, during some optical measurements a reddish FE glow in-between the electrodes was seen — even with bare eyes. This glow was seen at voltages *lower* than the breakdown voltage in both breakdown modes. In *spark cycle mode* the glow was always short, since once the capacitor is discharged, there is no longer energy supplied to the electrodes. On the contrary, in *breakdown rate mode* the glow was

sustained for as long as the power supply stayed connected with the electrodes (i.e. as long as switch S3 was closed). This was also tested at breakdown voltages, and the breakdown was always immediate, and no more breakdowns occured, although the reddish glow was sustained. This reddish glow is further discussed elsewhere by Kovermann et al. [31].

3.2 Sample preparation

Breakdowns are intentionally generated in the DC setup in the gap between a high voltage (HV) connected anode (tip) and a grounded cathode (plate) as shown in Fig. 2.1. Both electrodes are isolated from their holders by ceramic parts, and the anode is fixed in a special leverage system of sapphire spheres, allowing fine gap adjustments with µm precision.

For all experiments reported here, identical polycrystalline materials were chosen for both the anode and the cathode. The cathode samples are planar milled sheets of 2 mm thickness, and the anode samples are 2.3 mm thick rods with 1.15 mm tip radius. The electrode gap d is typically 20 µm.

The materials tested are milled copper (Cu OFE, UNS C10100) and molybdenum (Goodfellow MO000420), both with a purity > 99.9 %. The samples are always cleaned according to the CERN standard procedure for UHV components [32] prior to being installed in the UHV chamber. For the energy dependence study, milled Cu and Mo specimens (cf. Tab. 3.2) were tested in *spark cycle mode* with 2–3 spots for each capacitor (cf. Tab. 3.1), each spot with about 80–250 sparks. Results are discussed in Sec. 4, and a full overview of the testing of Cu and Mo is given in App. A.

Table 3.2: Different Cu and Mo specimens examined in this work, with their respective surface treatments and measurements. Specimen Cu7, Mo6, and Mo10 have a milled surface with the oxide layer naturally present after storage in air. Mo9 and Mo11 has a reduced oxide layer, and was not used to study the energy dependence.

Specimen	Surface state	Measurements
Cu7	Milled (slightly oxidized surface)	Spark cycle mode with β, dependence with energy
Mo6	Milled (oxidized surface)	Spark cycle mode with β, dependence with energy, single sparks, and preconditioning
Mo10	Milled (oxidized surface)	Spark cycle mode with β, dependence with energy and preconditioning
Mo9	Electropolished (slightly oxidized surface)	Spot evolution, spark cycle mode with β
Mo11	Electropolished and heat treated; 2 h, 1000 C, UHV furnace (nearly oxide-free surface)	Spot evolution, spark cycle mode with β

In addition, the evolution of the conditioning phase of Mo was examined in detail on two surface treated samples, both samples (Mo9 and Mo11) have an electropolished surface, in addition the Mo11 has undergone a 2 h heat treatment at 1000 °C in a Nb UHV furnace. The

heat treatment almost fully removes the oxide layer, which is confirmed by X-ray Photoelectron Spectroscopy (XPS) [33]. This method was also used by Ramsvik et al. to remove the oxide layer from Mo samples, it was then found that the oxide layer reappear fully within 8 hours in air [19]. The Mo11 sample spent about 1 hour in air while moving from the furnace to the pumping was completed in the spark test system.

The removal of the oxide allows the direct examination of the pure metal. The electropolishing step is necessary because it was found that the milled surface is quite rough, and complicates the subsequent localization of sparked areas with a scanning electron microscope (SEM). This became particularly pronounced for single sparked areas.

3.3 Corrections and error handling

For the many statistics produced by a spark cycle, the averages and deviations are handled in standard manners, including the *Student's dilatation factor* [34] for averages of less than 10 measurements. Unfortunately, even Superman has some weaknesses, and this section discusses how some of the weaknesses of the DC spark system are handled.

For long breakdown measurement runs, the gap distance is measured only every 5 to 50 breakdowns. For any change of the initially measured gap (d_i), the real gap (d_r) at each breakdown is linearly interpolated from the final gap value (d_f). This gives the following correction factor:

$$\begin{aligned} f_d &= \frac{d_i}{d_r} \\ d_r &= d_i + \frac{n_i}{n_{tot}} (d_f - d_i) \end{aligned} \tag{3.1}$$

where n_i is the the number of breakdowns since the last gap measurement and n_{tot} is the total number of breakdowns between the last two gap measurements. This affects both the calculation of the breakdown field and β (see Eq. 3.4) in terms of the field, E, used in the Fowler–Nordheim equation (Eq. 2.4). For Cu and Mo these corrections are usually small, while for other materials e.g. W and Co, the gap changes can be up to $0.5d$ after only one spark [27].

When measuring the breakdown field, the voltage over the electrodes is equal to the voltage from the power supply as long as C_1 is significantly higher than C_2. As we go to lower capacitances with C_1, the difference between the two capacitors decreases. From the circuit diagram (Fig. 3.1) we can derive the following relation to correct the voltage over the electrodes V_d due to the charging of C_2, giving another correction factor:

$$\begin{aligned} V_d &= f_C V_0 \\ f_C &= \frac{1}{1 + \frac{C_2}{C_1}} \end{aligned} \tag{3.2}$$

where V_0 is the nominal voltage from the power supply. As stated above, this implies that V_d is equal to V_0 when $C_2 \ll C_1$. This does not affect the β measurements, because C_1 and C_2 is not connected during a FE scan (cf. Fig. 3.1).

As seen in Fig. 3.1, a high voltage (HV) probe can be connected to measure the voltage over the electrodes. This is a new feature in DC system II. The HV probe has mainly been

used to gather information about the time constant of the voltage drop in the system and occasionally, to verify that a breakdown is occurring. Whenever connected, the HV probe always draws some current, meaning that a significant part of the energy stored in C_1 can go to ohmic losses in the the HV probe, while C_2 is charged.

When the HV probe is connected during β measurements the correction factor for the voltage which is used to calculate the field in the Fowler–Nordheim equation (Eq. 2.4) is:

$$\begin{aligned} V_{d,p} &= f_p V_0 \\ f_p &= \frac{1}{1 + \frac{R_{ext}}{R_p}} = \frac{1}{1.4} \end{aligned} \tag{3.3}$$

where the two resistances R_{ext} and R_p are the resistance marked 40 MΩ in Fig. 3.1 and the resistance of the HV probe = 100 MΩ, respectively. The influence on E_b from the HV probe in breakdown mode is not equally trivial to determine, and cannot be written into analytical form. The circuit has been simulated in the program LTSpice IV from Linear Technologies and showed that the corrections are negligible, hence no correction will be applied for this case [35].

Summarizing the corrections presented in this section, the corrected breakdown field E_b and the corrected field enhancement factor β is in total:

$$\begin{aligned} E_b &= f_d f_C \frac{V_0}{d_i} \\ \beta &= \frac{\beta_{meas}}{f_d f_p} \end{aligned} \tag{3.4}$$

where β_{meas} is the measured value, f_d is the correction for the gap being changed by breakdowns, f_C is the correction of the voltage over the electrodes due to small capacitance difference, and f_p is the correction factor for β if the HV probe has been connected during testing. These corrections are of course included in the calculation of the local breakdown field $E_{loc} = \beta E_b$.

4 Results

In this section the different breakdown parameters are presented as a function of the energy available for the breakdown. The energy is given by the capacitance, as defined in Eq. 2.7, where the applied voltage, V, is the average breakdown voltage of 2–3 series of 80–250 sparks per series, with the specific capacitor. The change in the breakdown voltage gives rise to the uncertainty seen for the energy in this section (see also Tab. 4.1). The uncertainty of the capacitances are negligible.

For the different capacitors C_1, the corresponding energy is shown in Tab. 4.1. For the energies $\lesssim 2$ mJ (equivalent to $C_1 \leq 0.1$ nF), the capacitance of C_1 matches the capacitance of the whole system, thus effectively we cannot decrease the energy further in the current DC spark setup, and the energy is no longer defined by Eq. 2.7. This will be further discussed in Sec. 5.1.

Table 4.1: Available capacitances for the DC system II, with corresponding energies for Cu and Mo, Mo is shifted to higher energies due to the higher breakdown field it sustains (cf. Sec. 4.2). Note that the corresponding energies of the the two lowest capacitances have been left out (cf. Sec. 5.1).

C_1 [nF]	27.5	15	2	0.56	0.1	0.01
W [mJ] (Cu)	45 ± 9	33.9 ± 0.6	6.6 ± 0.6	2.5 ± 0.9	—	—
W [mJ] (Mo)	441 ± 9	190 ± 110	17 ± 4	4.9 ± 0.8	—	—

The data sets presented in this section are corrected with the appropriate factors given in Sec. 3.3 unless otherwise stated. The complete series of conditioning curves for Cu and Mo are presented in App. B and C, respectively. In addition, the main results of those presented in this section, are also summarized in Fig. D.1 in App. D.

For a plot showing a breakdown parameter as a function of energy, the parameter itself is an average of 2–3 full conditioning curves (the conditioning phase excluded), and the errors are calculated as the standard deviation between these curves, including the *Student's dilatation factor* (cf. Sec. 3.3). Moreover, each of the conditioning curves consists of 80–250 sparks (including the conditioning phase), as can be seen in the appendices mentioned above.

4.1 Spot morphology

The confined area of surface damage from DC breakdowns is roughly a circular area, and an example of the spot diametre of such an area with estimated uncertainty, measured in SEM, is shown in Fig. 4.1. The spot diametres for Cu and Mo are shown as a function of energy in Fig. 4.2. For both materials the spot diametre increases with increasing energy.

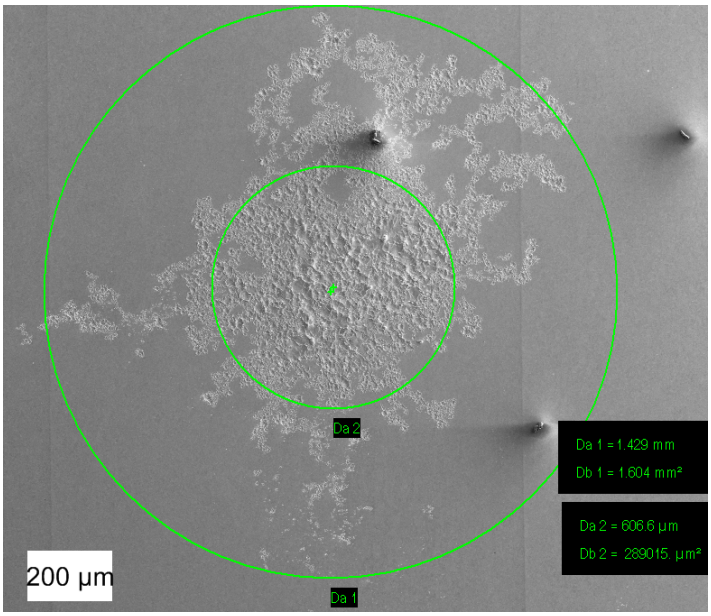

Figure 4.1: A spot diametre is taken as $d = \frac{1}{3}d_{outer} + \frac{2}{3}d_{inner}$, where the inner circle contains at least 95 % resolidified surface, and the outer circle is as indicated (including almost every trace of splashes). The uncertainty is taken as half the difference between the outer and inner diametre. [36]

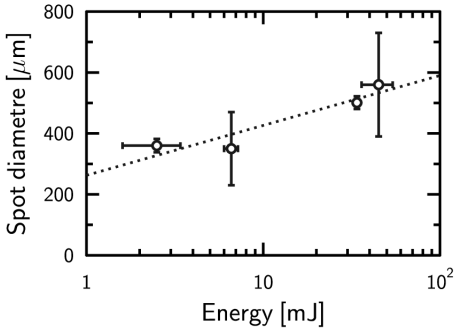

(a) Cu [37]

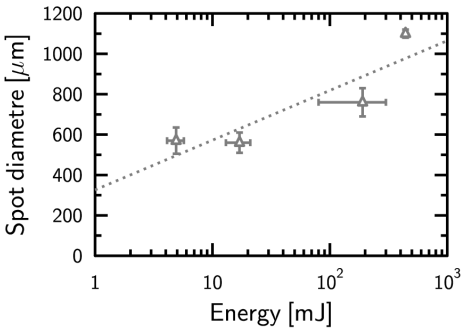

(b) Mo [38]

Figure 4.2: Spot diametre for (a) Cu and (b) Mo as a function of energy. For both, the spot size is increasing with increasing available energy.

Qualitative investigation with SEM revealed deeper craters at the highest energies, meaning that more material has been molten. For the lower energies the craters are quite shallow and less fingerlike structures (i.e. molten splashes) are formed, see Fig. 4.3. The surface is altered less — by conditioning or deconditioning — when less energy is available for breakdown.

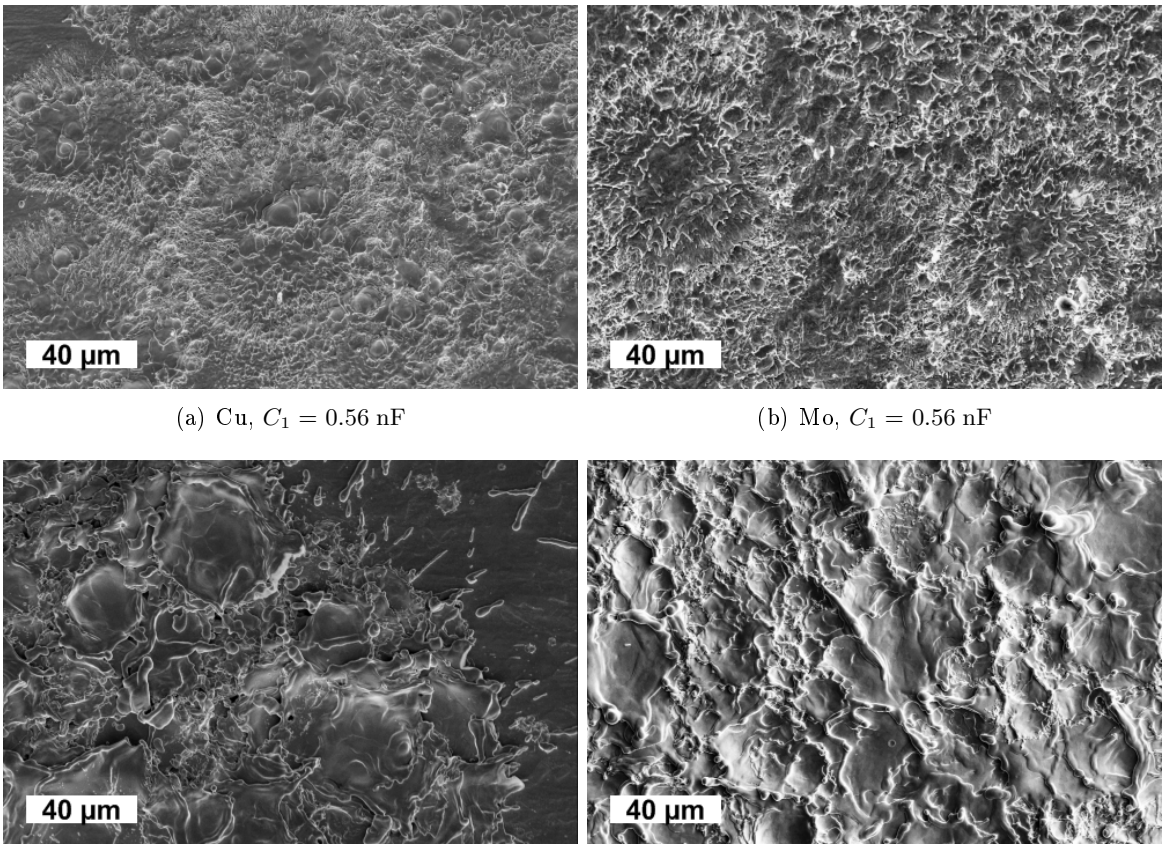

(a) Cu, $C_1 = 0.56$ nF (b) Mo, $C_1 = 0.56$ nF

(c) Cu, $C_1 = 27.5$ nF (d) Mo, $C_1 = 27.5$ nF

Figure 4.3: Qualitative difference in spot morphology at different energies. For low energies (a)-(b) the craters are significantly shallower than the craters at the high energies (c)-(d). The two pictures from Cu are taken on the edge of a spot, so one can see a difference in the amount of material sputtered away from the craters. Pictures are taken by P. Alknes and A. Toerklep [37, 38].

This difference between deep and shallow craters as a function of energy corresponds with the theoretical observation from the molecular dynamics (MD) modelling of the DC breakdown. It was found that to form deep craters, it is necessary to melt the whole volume in which the energy deposition takes place. As a consequence, when the energy is large enough, ion bombardment events overlap, deep craters are formed and clusters are sputtered. For energies below a certain threshold mostly single atoms — and not clusters — are sputtered from the cathode. [39]

4.1.1 Evolution of spot size with number of sparks for Mo

The surface damage evolution caused by $1, 5, 10, 20$, and 40 sparks has been investigated, on the samples Mo9 and Mo11 (cf. Tab. 3.2). Each test was made on a new, undamaged area,

twice on each sample. The motivation for inspecting this closer was the fact that the spot sizes presented in Sec. 4.1 are *independent* of the total number of sparks (ranging from $\sim$ 80–250 sparks). The full spot diametre of $\sim$ 1000–1100 µm (see Fig. 4.2(b)) is achieved in about 40–50 sparks only, regardless of the sample preparation and the oxide layer thickness. The typical spot development for Mo is presented in Fig. 4.4 and is visualized with micrographs in Tab. 4.2.

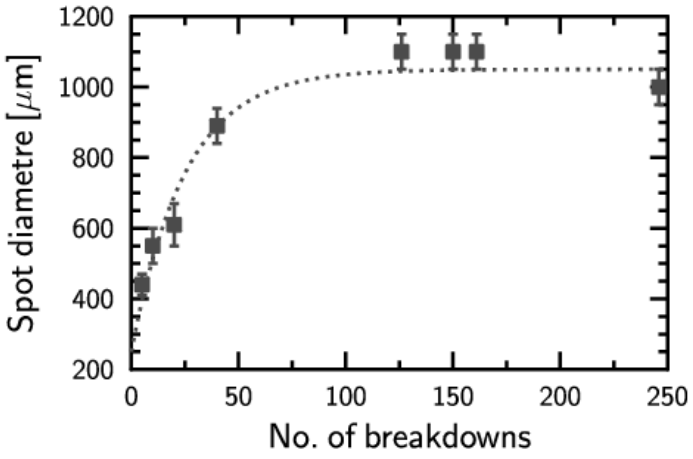

Figure 4.4: Evolution of spot diametre (D) for Mo with the number of sparks (n). The spot is growing until $\sim$ 50 sparks, which is coinciding with the length of the conditioning phase. These measurements are all with $C_1 = 27.5$ nF. The function drawn to illustrate the tendency corresponds to the function $D = 250 + 800\,(1 - exp(-n/25))$

An oxide free sample does not exhibit conditioning, since we immediately measure on bulk material. Nonetheless, the spot takes about 40–50 sparks to grow. However, if there is an oxide layer on the sample, the breakdown field will steadily grow with the evolution of the spot size, see Fig. 4.4. This is because some unsparked, oxide covered areas are still present within the area of the final spot and the molybdenum oxide has a lower breakdown field than pure Mo. When the oxide is removed from the area of the entire spot and the final spot size is reached, also the breakdown field saturates (cf. Sec. 4.2). Therefore, Mo conditions within 30–50 sparks. This is further discussed in Sec. 5.2.

4.2 Conditioning curve and saturated field

The duration of the conditioning phase with a conditioned anode and a virgin cathode surface, as discerned from the conditioning curves, does not vary much with energy. For Cu a very short *de*conditioning phase of about 2–8 sparks is present, see Fig. 4.5. For Mo the conditioning phase is approximately 40 sparks over the entire energy range tested, see Fig 4.6. The effect of the energy on the conditioning phase is further discussed in Sec. 4.2.1.

The saturated field, i.e. the breakdown field reached after conditioning, changes with the available energy, see Fig. 4.7(a). For Cu, E_{sat} is found to decrease with increasing energy. This could be expected since Cu exhibits deconditioning, meaning the lower the energy available for breakdown, the less effective the deconditioning is, thus a higher E_{sat} is obtained.

For Mo, the opposite tendency is seen, E_{sat} increases slightly with increasing energy, see

Table 4.2: SEM micrographs of the development of Mo spot size as a function of sparks on two samples (Mo9 and Mo11) with different surface treatments, both measured with $C_1 = 27.5$ nF. Note the different length scales in the pictures. Pictures are taken by P. Alknes [36, 40].

No. of sparks	Electropolished Mo	Electropolished, heat treated Mo
1	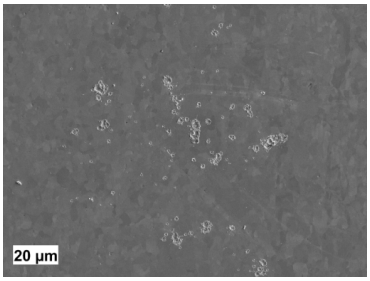	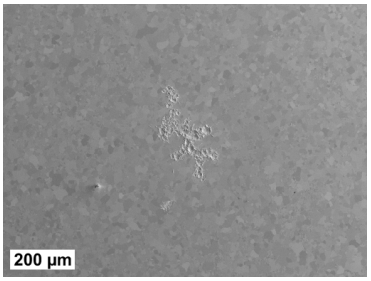
5	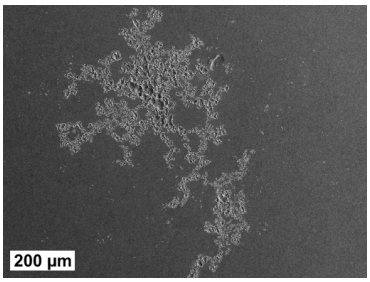	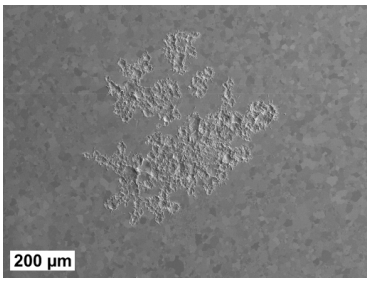
10	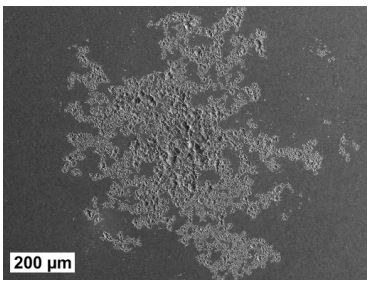	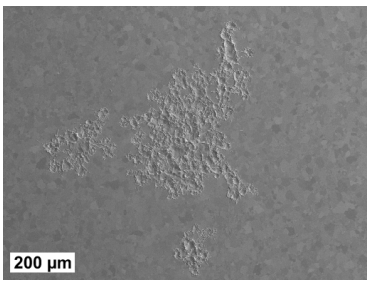
20	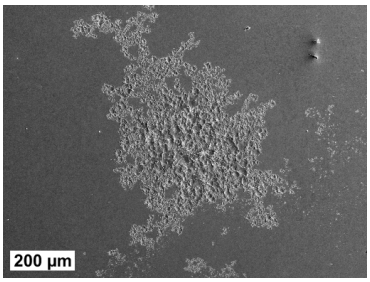	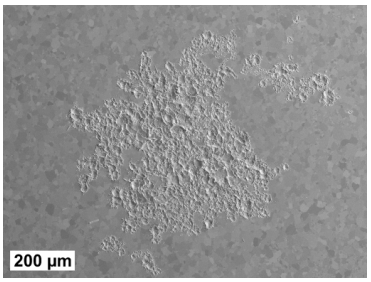
40	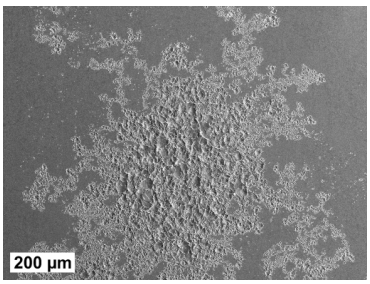	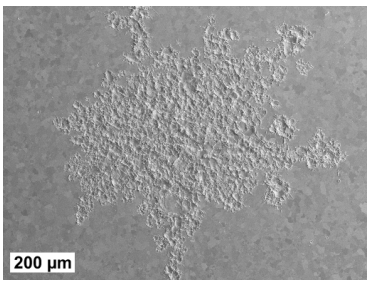

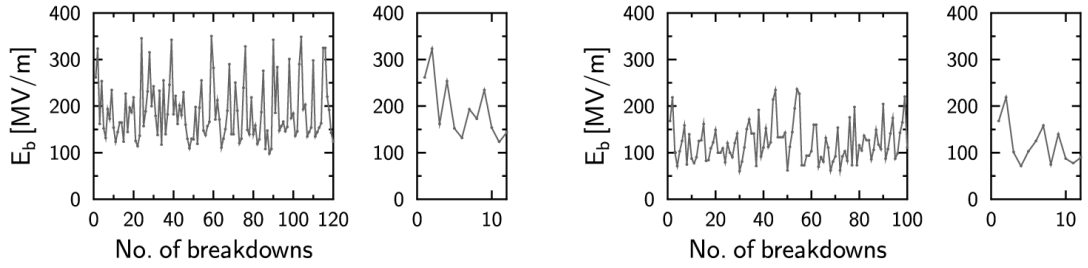

Figure 4.5: (a), (c): Conditioning curves for **Cu** at different capacitances; (a)–(b) $C_1 = 2$ nF, $E_{sat} = (190 \pm 60)$ and (c)–(d) $C_1 = 27.5$ nF, $E_{sat} = (120 \pm 40)$. (b) and (d) show the first 12 sparks of curves (a) and (c), respectively. Deconditioning can be seen for both of these ((b) and (d)), and the saturated field is decreasing with increasing energy (capacitance). The uncertainty of the saturated field is here simply the full fluctuations of the breakdown field.

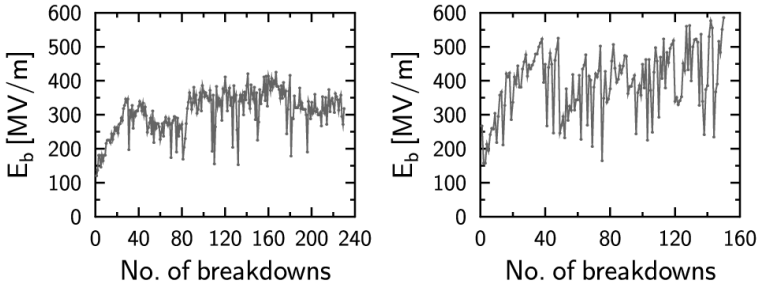

Figure 4.6: Conditioning curves for **Mo** at (a) $C_1 = 2$ nF, $E_{sat} = (320 \pm 50)$ and (b) $C_1 = 27.5$ nF, $E_{sat} = (400 \pm 60)$. The conditioning speed for the different capacitances remains constant around ~ 40 sparks, however, the saturated field increases with increasing energy. The uncertainty of the saturated field is here simply the full fluctuations of the breakdown field.

Fig. 4.7(b). Since Mo conditions, this indicates also a "softer" (less effective) conditioning, meaning that the lower energy that is available is not enough to condition to such high fields as what was normally seen (i.e. at $C_1 = 27.5$ nF) for Mo.

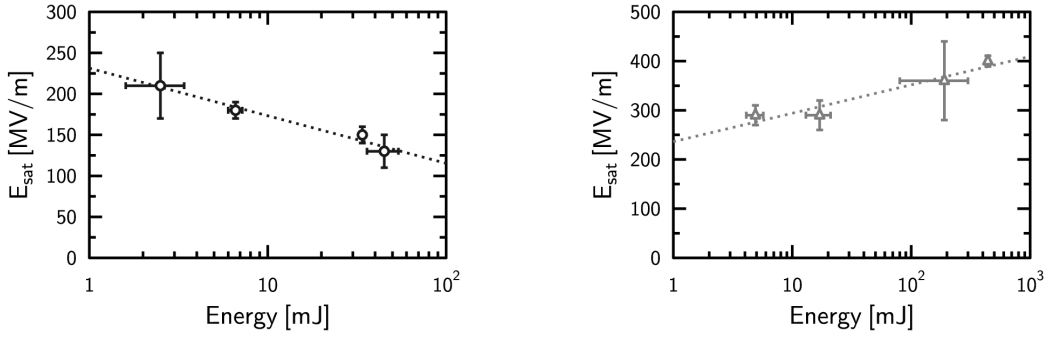

(a) Cu (b) Mo

Figure 4.7: Saturated breakdown field for (a) Cu and (b) Mo as a function of energy. E_{sat} decreases with increasing energy for Cu and increases for Mo.

4.2.1 Preconditioning of Mo

To further investigate the effect of the conditioning on the saturated field, so-called *preconditioning* tests have been carried out for Mo. The idea is to condition with high capacitance (27.5 nF), i.e. with high energy, and then measure the saturated field with lower capacitance. This was done by two different approaches:

(i) To condition in *spark cycle mode*.

(ii) To condition in *breakdown rate mode*, meaning that the surface is sparked at breakdown rate 1 (100 % breakdown probability), here for 20 sparks, before continuing in *spark cycle mode*.

Interestingly, these two approaches gave different results:

(i) When conditioning for 40 sparks with the 27.5 nF capacitor in *spark cycle mode*, the obtained E_{sat} measured with the 2 nF capacitor was (400 ± 70) MV/m. Whereas for the usual conditioning curves, in which the *full run* is performed with the 2 nF capacitor, $E_{sat} = (290 \pm 50)$ MV/m is obtained.

(ii) For conditioning in *breakdown rate mode*, the 27.5 nF capacitor was used with the field fixed at 500 MV/m, which is sufficiently high to cause breakdown at each of the 20 attempts, i.e. the breakdown rate is 1. Subsequently measuring the saturated field in *spark cycle mode* with the 0.56 nF capacitor, gives an $E_{sat} = (330 \pm 60)$ MV/m, which is about the same saturated field as obtained for the usual conditioning run using only the 0.56 nF capacitor, which is $E_{sat} = (290 \pm 50)$ MV/m. Nonetheless, it is possible that if more than 20 breakdowns had been carried out in *breakdown rate mode* as the preconditioning, this spot could also have saturated at a higher field, giving the same result as the first method.

The first method shows that there is a strong correlation with the energy available for conditioning and the saturated field which can be obtained afterwards, which is the same result as shown in Fig. 4.7 for both Cu and Mo.

4.3 Field enhancement factor and local field

The typical evolution of β in spark cycle mode is shown for Mo and Cu in Fig. 4.8(a) and 4.8(b), respectively. For Mo, β varies within 20 and 60, while for Cu, β is on average higher than Mo, and varies from 30 to 120. The first β, measured on an undamaged surface before the first spark, and the following 1–2 β measurements are often lower than the average β. This could be because the surface is smoother, so no dominating field emitters are produced yet and that the naturally present surface oxide layer affects the first β measurements.

The effect on the β measurements when the HV probe is connected, is shown for the uncorrected Cu data in Fig. 4.8(c): the average β value decreases (compared to Fig. 4.8(b)), due to the effects to be corrected for as described in Eq. 3.3. In addition, the presence of the HV probe noticeably influences the fluctuation of β: changing from ± 45 % without the probe to ± 30 % with the probe.

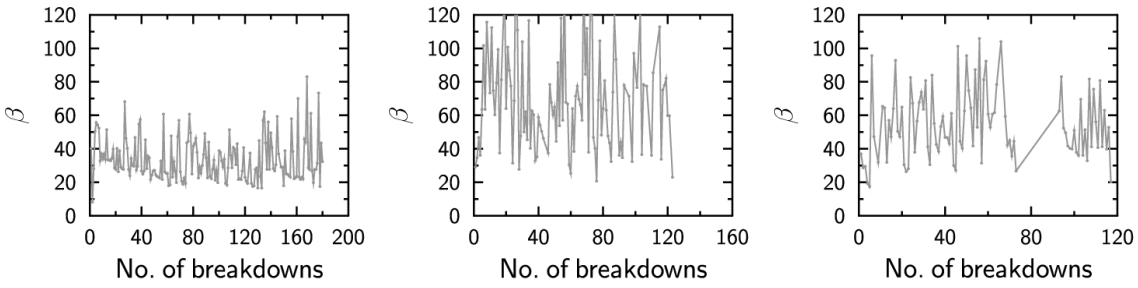

(a) Mo (b) Cu (c) Cu, *with HV probe*

Figure 4.8: Typical evolution of β for (a) Mo and (b) Cu with the conditioning curve. (c) The influence from the HV probe on β for Cu; the average β value is decreased compared to (b), and needs to be corrected with the correction factor f_p (cf. Eq. 3.3). β is not measured in the interval 75–95 breakdowns. Note that the presence of the HV probe influences the fluctuation of β: changing from $\pm 45\%$ (without the probe) to $\pm 30\%$ (with the probe). (All these data were tested with $C_1 = 2$ nF).

The field enhancement factor, β, averaged over the conditioning curve (excluding the conditioning phase) is shown in Fig. 4.9. For Cu, the inverse tendency for β as for E_{sat} is seen (cf. Fig. 4.7(a)): β increases with increasing energy. In turn, this causes the calculated local field to be constant at (9.7 ± 0.9) GV/m, see Fig. 4.10(a).

For Mo, no tendency of β as a function of energy is seen, i.e. the average β is constant at 32 ± 2, see Fig. 4.9(b). This results in a similar tendency for E_{loc}, see Fig. 4.10(b), as we saw for E_{sat} (cf. Fig. 4.7(b)): increasing with increasing energy.

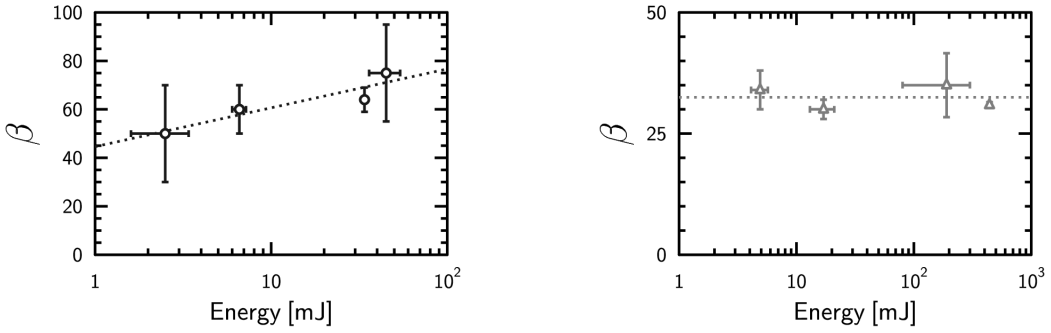

(a) Cu (b) Mo

Figure 4.9: Average β (after conditioning) for (a) Cu and (b) Mo as a function of energy. For Cu β increases with increasing energy, which is the inverse tendency as for E_{sat}. For Mo the average β is more or less constant at 32 ± 2.

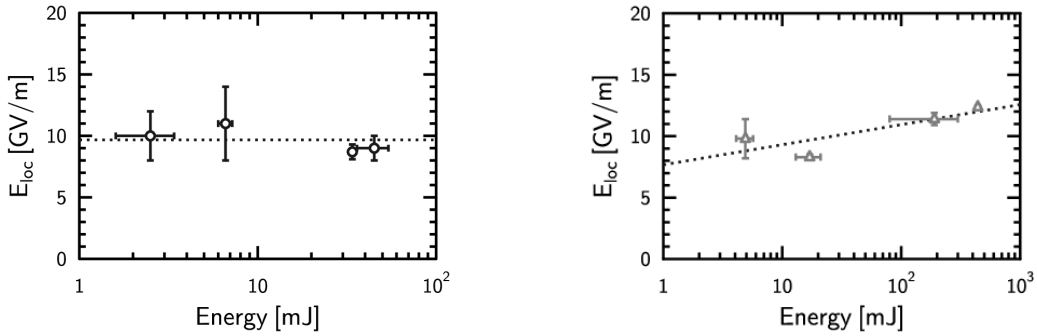

(a) Cu (b) Mo

Figure 4.10: Average E_{loc} (after conditioning) for (a) Cu and (b) Mo as a function of energy. The local field is constant for Cu at (9.7 ± 0.9) GV/m, and for Mo the same tendency is seen as for E_{sat}, an increasing local field with increasing energy.

.

5 Discussion

5.1 System limitations

Even though it was known that there would be a lower limit of the energy for feasible testing in the DC setup, additional experiments were carried out with $C_1 = 0.01$ and 0.1 nF (theoretically corresponding to an energy in the order of 0.1 to 1 mJ) for both materials. At this level the capacitance of the whole system is already comparable to C_1, thus these results are unreliable. One indication for this is that large oscillations are seen in the discharge current, see Fig. 5.1(a). Even more striking is the fact that all measured breakdown properties saturate to more or less the same values as measured with $C_1 = 0.56$ nF, see the example in Fig. 5.1(b).

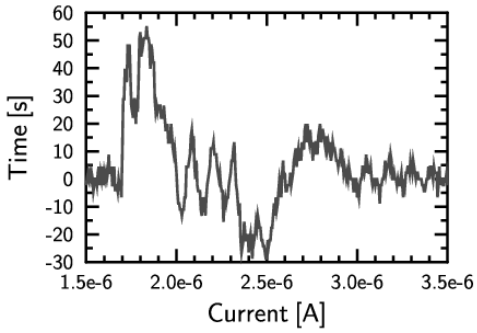

(a) Oscillating discharge current at $C_1 = 0.1$ nF, indicating that the limits of the system are reached.

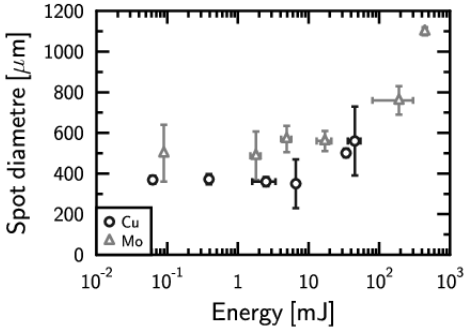

(b) Saturation of spot diametre at energies supposedly below 2 mJ. The real energy dissipated through the breakdown is no longer known as C_1 is comparable to the capacitance of wires etc.

Figure 5.1: Energy limitations of the DC spark setup.

5.2 DC conditioning and field enhancement factor

In Sec. 4.1.1 an explanation has been suggested for the DC conditioning mechanism. In the case of Mo it is easily seen that, for Mo with an oxide layer, conditioning lasts as long as the spot is growing, meaning until all unsparked, oxide covered areas become sparked. In order to generalize this mechanism to other materials, the mechanism needs to be verified by testing several materials. Since Cu does not condition for a long number of sparks, it could be expected that a spot on Cu grows quicker, i.e. that the sparked area after one breakdown

is larger than for Mo, or that the less stable oxide layer on Cu is removed also on areas next to the spot. Ongoing work with single sparks on Cu, by Hansen et al. [41], will discuss this matter further.

At lower energies the conditioning becomes "softer" (i.e. less effective). This is the reason why the saturated field (E_{sat}) scales with energy, as described in Sec. 4.2. This scaling is possible if some surface properties are different when testing at different energies, for instance, possibly a higher oxide fraction remains on the less conditioned surface, since the surface damage is shallower. As β characterizes the surface properties, it should also reflect this difference.

The different surface properties can explain how it is possible that β changes with energy (as seen for Cu), even though changing C_1 does not affect the circuit during β measurements. The difference between the two materials, with the field enhancement factor scaling with energy for Cu and being constant for Mo, could be due to the whisker growth abilities to form more easily in Cu, due to fcc crystal lattice, than in the bcc lattice of Mo. For the time being, this is a not yet proven but an interesting theory, so it should be taken into consideration in future investigation of breakdowns.

In *spark cycle mode*, as explained in Sec. 3.1.1, β is currently measured only prior to the voltage ramp-up, and not in-between each step of the ramp-up. Considering that field emitters — like whiskers — can grow during this ramp-up, the values measured for β might not be the same as that actually present just before breakdown. If it is the case that the actual β at breakdown is not measured, then also the calculated local field at breakdown is wrongly estimated, and can only be used as a relative value for comparison between similar experiments and not as an absolute value. However, there is a huge dynamic range between the FE current for β measurements ($\sim$ pA–nA) and the discharge current (10–100 A), thus these can not be measured with the same device. To protect the measurement apparatus β measurements are limited to low FE currents. Therefore, by the present means of the setup, the we can not measure the field emission current directly prior to breakdown.

5.3 A criterion for breakdown

Descoeudres et al. [23] observed, when testing Cu in breakdown rate mode, that the repeated application of high enough fields without breakdowns leads to an increasing β. The structures causing the increase are stable even after switching off the field, and β continues to increase when the field is applied once more. At lower fields, these structures may not be stable, and β is seen to decrease (cf. Fig. 2.2), the surface protrusions are possibly diminished by field induced stress release. These two processes, the increase and decrease of β, might both be explained by the whiskers growth theory, as introduced in Sec. 2.3.

The experiments mentioned above by Descoeudres et al. suggest that there is a limiting local field, βE. If any field emitter combined with the external applied field exceeds this limit, a breakdown seems to occur. This was also one of the most important assumptions in work of the DC spark statistical modelling by Levinsen et al. [9], and is consistent with early literature [42]. This means that for Cu, the growing β could be used as a warning for the next breakdown. Tests could be made to see a practical use of this, for instance whether inducing a breakdown at an earlier stage (by increasing the voltage) when β is already growing, would decrease the breakdown probability for the remaining of that run.

From the current work, it is interesting to see that the local field at breakdown is constant (for Cu) at all the energies tested. Note that in this work the *spark cycle mode* has been used, which is different from the *breakdown rate mode*. It is seen in the results of Descoeudres et al. (cf. Fig. 2.2) that the values of β are considerably higher in a period of consecutive breakdowns, than β in quiet periods and the β required for discharging. The *spark cycle mode* corresponds to a period of consecutive breakdowns in *breakdown rate mode*, and it is therefore expected that the *spark cycle mode* gives an upper limit of the local breakdown field. Nonetheless, the values for the local field do not differ much (for Cu) between these two modes.

Since the local field is constant over the energy range for Cu, and seems to be a criterion for breakdown, it raises the question about the local field being a material parameter. Contradictory to this, the local field is not constant over the energy range for Mo. Breakdown rate experiments with monitoring the evolution of β have not yet been done for Mo, so conclusions can not be drawn at the time, however, a similar behaviour as for Cu, with increasing or decreasing β at various fields, is expected also for Mo.

5.4 Further work

To complete the work on energy scaling of breakdown properties, one remaining part is to examine how the energy influences breakdown probability, i.e. breakdown rate measurements. Another important experiment is to do breakdown rate measurements on Mo, while monitoring β, to see if some conclusions can be drawn on using the local field with the growing β as a criterion for breakdown. Further, as mentioned in the previous section, tests should be made to see if *inducing* a breakdown when β is growing, would decrease (or even increase) the breakdown probability.

General improvements for the DC system could also be made. One is to implement another switch in the electronics, in order to use the HV probe without having to correct the β measurements in *FE mode*. Another is to be able to measure β in-between each voltage step in the ramp-up when testing in *spark cycle mode*. The impedance of the DC setup, including wires etc., should be optimized for the energies the system will continue to operate at, this will also contribute to determining the true limits of the system.

It was stated by Djurabekova et al. [24] that experimentally no whiskers have been seen to occur at $T > 90$ °C. The DC setup can be rebuilt to achieve this, and running breakdown rate measurements at these elevated temperatures, could result in less growth or even no growth of β. In addition, since dislocations hardly move at very low temperatures, it was proposed by K. Nordlund [43] that it would be interesting to see the effect of the applied field on β when going down to liquid nitrogen temperatures. A new sample holder for the DC spark system to test at elevated and lowered temperatures is underway.

6 Conclusions

The energy dependence of breakdown properties has been examined for two materials, Cu and Mo. Cu has shown a very short *de*conditioning phase of 2–8 breakdowns, while Mo has a conditioning phase of 30–50 sparks. The length of the conditioning phase, for both Cu and Mo, does not change with the energy available for breakdown. Mo is found to condition as long as the diametre of the surface damage on one spot is growing. This is correlated to the removal of the initial surface, i.e. the oxide layer, dust, impurities, etc., within the spot. A spot needs about 50 breakdowns to spark the total area (at least once) of the spots full size.

The full spot diametre, measured after 100–250 sparks, is related to the energy available for breakdown and not the total number of breakdowns. The full spot size increases with increasing energy for both Cu and Mo. The surface damage craters were qualitatively observed to be significantly shallower at the low energies tested (1 mJ) than at the higher energies $0.1 - 1$ J.

The saturated field, reached after (de)conditioning, decreases for Cu and increases for Mo with increasing energy. This is attributed to the (de)conditioning being more effective at higher energies. The field enhancement factor increases with increasing energy for Cu, and is constant (at 32 ± 2) for Mo. This results in a constant local field for Cu (at 9.7 ± 0.9 GV/m), which is within the range of earlier reported values [23]. On the other hand, for Mo, the calculated local field increases with increasing energy.

With this work an important and big step towards mapping breakdown properties as a function of energy has been made. The energy limitations of the system have been identified. Also, a better understanding of the conditioning process seen in DC has been gained. The missing piece to fulfil the work of the energy dependence, is examining the breakdown probability as a function of energy. All the knowledge coming from the presented work will ease the work of fitting the last piece of the puzzle.

Bibliography

[1] H. Braun, J.-P. Delahaye, A. De Roeck, and Günther Geschonke. The Compact Linear Collider study aims for the high-energy frontier. *CERN Courier*, 48, Number 7:15–18, 2008.

[2] W. Wunsch. Progress in understanding the high-gradient limitations of accelerating structures. In *Proceedings of the 4th Asian Particle Accelerator Conference, Indore, 2007 (RRCAT, Indore, India, 2007)*, page 544, 2007.

[3] H. Braun, R. Corsini, J.-P. Delahaye, A. De Roeck, S. Doebert, G. Geschonke, A. Grudiev, C. Hauviller, B. Jeanneret, E. Jensen, T. Lefevre, Y. Papaphilippou, G. Riddone, L. Rinolfi, W.-D. Schlatter, H. Schmickler, D. Schulte, I. Syratchev, M. Taborelli, F. Tecker (editor), R. Tomás, S. Weisz, and W. Wunsch. CLIC 2008 parameters. CLIC-Note-764, 2008.

[4] J. Ellis and I. Wilson. New physics with the Compact Linear Collider. *Nature*, 409:431–435, 2001.

[5] W. S. Boyle, P. Kisliuk, and L. H. Germer. Electrical Breakdown in High Vacuum. *J. Appl. Phys.*, 26(6):720–725, 1955.

[6] S. Döbert, A. Grudiev, G. Riddone, M. Taborelli, W. Wuensch, R. Zennaro, S. Fukuda, Y. Higashi, T. Higo, S. Matsumoto, K. Ueno, K. Yokoyama, C. Adolphsen, V. Dolgashev, L. Laurent, J. Lewandowski, S. Tantawi, F. Wang, and J.W. Wang. High power test of a low group velocity X-band accelerator structure for CLIC. In *Proceedings of LINAC08*, pages 930–932, Canada, 2008.

[7] M. Kildemo. Breakdown and field emission conditioning of Cu, Mo, and W. *Phys. Rev. ST Accel. Beams*, 7, 2004.

[8] M. Gerbaux, S. Dobert, J. Kovermann, I. Syratchev, and R. Zennaro. Results of the 30 GHz high power RF test on the Speed Bump and TM02 structures. (submitted for publication), 2009.

[9] Y.I. Levinsen, A. Descoeudres, S. Calatroni, M. Taborelli, and W. Wuensch. Statistical modeling of DC sparks. In *Proceedings of PAC 2009*, volume TU5PEP012, 2009.

[10] Richard G. Forbes. Field evaporation theory: a review of basic ideas. *Appl. Surf. Sci.*, 87-88:1 – 11, 1995. Proceedings of the 41st International Field Emission Symposium.

[11] M. Vesely and G. Ehrlich. Field evaporation: Model and experiment. *Surf. Sci.*, 34:547–560, February 1973.

[12] H. Timkó, K. Matyash, R. Schneider, F. Djurabekova, K. Nordlund, A. Hansen, A. Descoeudres, J. Kovermann, A. Grudiev, W. Wuensch, S. Calatroni, and M. Taborelli. A one-dimensional Particle-in-Cell model of plasma build up in vacuum arcs. (submitted for publication), 2009.

[13] H. Padamsee, J. Knobloch, and T. Hays. *RF Superconductivity for Accelerators*. Wiley Series in Beam Physics and Accelerator Technology, 1998.

[14] K. L. Jensen, Y. Y. Lau, D. W. Feldman, and P. G. O'Shea. Electron emission contributions to dark current and its relation to microscopic field enhancement and heating in accelerator structures. *Phys. Rev. ST Accel. Beams*, 11(8):081001, Aug 2008.

[15] R.G. Forbes. Refining the application of Fowler-Nordheim theory. *Ultramicroscopy*, 79:11–23(13), September 1999.

[16] J. W. Wang and G. A. Loew. Field emission and rf breakdown in copper linac structures. *Part. Accel.*, 30(SLAC-PUB-5059):225–230, Aug 1989.

[17] J. Hölzl, F.K. Schulte, and H. Wagner. *Solid Surface Physics*, volume 85 of *Springer Tracts in Modern Physics*. Springer Berlin / Heidelberg, 1979.

[18] H. Timko, F. Djurabekova, K. Nordlund, K. Matyash, and R. Schneider. Breakdown simulation update, 2008. CLIC08 Workshop, `http://indico.cern.ch/contributionDisplay.py?contribId=162&confId=30383`.

[19] T. Ramsvik, S. Calatroni, A. Reginelli, and M. Taborelli. Influence of ambient gases on the DC saturated breakdown field of molybdenum, tungsten and copper during intense breakdown conditioning. *Phys. Rev. ST Accel. Beams*, 10, 2007.

[20] A. Descoeudres, T. Ramsvik, S. Calatroni, M. Taborelli, and W. Wuensch. DC breakdown conditioning and breakdown rate of metals and metallic alloys under ultrahigh vacuum. *Phys. Rev. ST Accel. Beams*, 12, 2009.

[21] W. Wuench. Personal contact, 2009. DC breakdown progress meeting.

[22] S. Calatroni. Personal contact, 2009. DC breakdown progress meeting.

[23] A. Descoeudres, Y.I. Levinsen, S. Calatroni, M. Taborelli, and W. Wuensch. Investigations of DC vacuum breakdown mechanism. *Phys. Rev. ST Accel. Beams*, 12, 2009.

[24] F. Djurabekova, H. Timko, A. Pohjonen, and K. Nordlund. Breakdown simulation update, February 25, 2009. CLIC RF structure development meeting, `http://indico.cern.ch/conferenceDisplay.py?confId=47633`.

[25] G. T. Gaylon. A history of tin whisker theory: 1946 to 2004. In *SMTAI International conference, (Chicago, IL)*, 2004. `http://thor.inemi.org/webdownload/newsroom/Presentations/SMTAI-04_tin_whiskers.pdf`.

[26] F. Djurabekova, H. Timko, A. Pohjonen, and K. Nordlund. Breakdown studies, 2009. CLIC09 Workshop, `http://indico.cern.ch/contributionDisplay.py?contribId=11&confId=45580`.

[27] A. Descoeudres, Y. Levinsen, A. Hansen, S. Calatroni, M. Taborelli, and W. Wuensch. Latest news of the DC breakdown experiments for CLIC, June 26, 2009. CLIC RF structure development meeting, `http://clic-meeting.web.cern.ch/clic-meeting/`.

[28] G. E. Dieter. *Mechanical Metallurgy — SI Metric ed.* McGraw-Hill, 3. ed. edition, 1988.

[29] L. J. Giacoletto, R. W. Landee, D. C. Davis, and A. P. Albrecht. *Electronics Designers' Handbook*, pages 9.48–9.51. McGraw-Hill Book Company.

[30] M. Kildemo. New spark-test device for material characterization. *Nucl. Instrum. Methods Phys. Res., Sect. A*, 530:596–606, 2004.

[31] J. Kovermann. Breakdown experiments, 2009. CLIC09 Workshop, `http://indico.cern.ch/contributionDisplay.py?contribId=146&confId=45580`.

[32] C. Scheuerlein and M. Taborelli. The assesment of metal surface cleanliness by XPS. *Appl. Surf. Sci.*, 252:4279–4288, 2005.

[33] D. Letant-Delrieux. Job No.: 2281-XPS-TE-VSC-CSA-2009-10-12. Technical report, CERN, EDMS 1035314, October 2009.

[34] K. Nordlund. Basics of Monte Carlo simulations. Course material, `http://beam.acclab.helsinki.fi/~knordlun/mc/mc5nc.pdf`, 2006.

[35] J. Kovermann. Personal contact, 2009.

[36] P. Alknes. DC spark — Mo 9. Technical report, CERN, EDMS 1031906, October 2009.

[37] P. Alknes. DC spark — Cu 7. Technical report, CERN, EDMS 1027679, September 2009.

[38] A. Toerklep. DC spark — Mo 6. Technical report, CERN, EDMS 1014830, September 2009.

[39] H. Timkó, F. Djurabekova, K. Nordlund, L. Costelle, K. Matyash, R. Schneider, A. Toerklep, G. Arnau-Izquierdo, A. Descoeudres, S. Calatroni, M. Taborelli, A. Toerklep, and W. Wuensch. Mechanism of surface modification from the arc plasma-surface interaction in Cu. (submitted for publication), 2009.

[40] P. Alknes. DC spark — Mo 11. Technical report, CERN, EDMS 1041699, October 2009.

[41] A. Hansen, H. Timkó, P. Alknes, A. Toerlep, M. Taborelli, S. Calatroni, A. Grudiev, W. Wuensch, K. Nordlund, and F. Djurabekova. Energy dependence of breakdown properties of Cu and Mo. (to be published), 2010.

[42] D. Alpert, D. A. Lee, E. M. Layman, and H. E. Tomaschke. Electrical Breakdown in High Vacuum. *J. Vac. Sci. Technol.*, 1:35–50, 1964.

[43] K. Nordlund. Personal contact, 2009. DC breakdown progress meeting.

Appendices

A Overview of measurements

The tables in this appendix gives an overview over the measurements carried out for the present work, and are included here as a reference to those who will continue to work with the DC setup.

Table A.1: Conditioning measurements with β measurements for copper, sample Cu7, standard milled and cleaned surface.

Spot no.	C_1 [nF]	C_2 [nF]	n_{tot}	D [µm]	HV probe	Comments
1	27.5	0.167	100	700 ± 200	Y	Unconditioned tip
2	27.5	0.167	125	470 ± 70	Y	
3	27.5	0.167	120	500 ± 90	Y	
4	15	0.167	(45+)	400 ± 110	Y	FAILED
5	2	0.167	117	410 ± 110	Y	
6	2	0.167	92	360 ± 50	Y	
7	0.56	0.167	(30+)	360 ± 60	Y	FAILED
8	0.1	0.004	(121+)	360 ± 130	Y	FAILED
9	0.1	0.004	100	380 ± 90	N	C_2 not connected
10	0.1	0.004	(10+)	180 ± 70	Y	FAILED: C_2 having breakdowns
11	0.56	0.167	131	350 ± 30	N	
12	0.1	0.004	110	360 ± 40	N	New $C_2 = 4$ pF
13	2	0.004	123	290 ± 50	N	Scope not cooperating
14	0.01	0.167	96+ 50	400 ± 40	Y&N	
18	15	0.167	100	500 ± 120	N	No β for the first 2-3 sparks, no pressure data
19	27.5	0.167	100	650 ± 130	N	No pressure data
20	0.01	0.004	92	—	N	FAILED: Spot on the edge of the sample

Table A.2: Conditioning measurements with β evolution for molybdenum, sample Mo6, standard milled and cleaned surface. Spot diametre uncertanty, unless given, is ± 20 µm.

Spot no.	Measurement mode	C_1 [nF]	C_2 [nF]	n_{tot}	D [µm]	HV probe	Comments
			Sample Mo6 — Milled surface				
1	Contitioning, new tip	27.5	0.333	264	850	N	Unconditioned tip, problems with FE measurements
2	Contitioning	27.5	0.333	126	1100	N	60 sparks without pressure data
3	Contitioning	27.5	0.333	150	1100	N	No pressure data
4	Contitioning	27.5	0.333	151	1100	N	No pressure data
5	Contitioning	15	0.333	151	870	N	No pressure data
6	Contitioning	15	0.333	180	690	N	No pressure data
7	Contitioning	15	0.333	162	730	N	No pressure data
8	Contitioning	2	0.333	230	570	N	No pressure data
9	Contitioning	2	0.333	180	500	N	No pressure data
10	Contitioning	2	0.333	231	610	N	70 last sparks without pressure data
11	Contitioning	0.56	0.167	150	480	N	
12	Contitioning	0.56	0.167	(n?)	450	N	FAILED
13	Contitioning	0.56	0.167	∼190?	530	N	FAILED
14	Contitioning	0.56	0.167	245	610	N	
15	Preconditioning in breakdown rate mode (27.5nF, 20sparks, 500MV/m), then conditioning mode	0.56	0.167	20+ 102	970	Y&N	HV probe not for the 5 first sparks after preconditioning
16	Contitioning	0.1	0.004	113	610	Y&N	HV probe not for the 10 first sparks
17	Contitioning	0.56	0.167	96	630	Y	
33	Preconditioning in contitioning mode (27.5nF, 40sparks), then conditioning	0.56	0.167	(40+ 30?)	900	Y	FAILED
34	Preconditioning in conditioning mode (27.5nF, 40sparks), then conditioning	2	0.167	40+ 20	950	Y	In the end, Eb too high to be measured: Vb>12kV, Eb>600MV/m
			Sample Mo10 — Milled surface				
1	Preconditioning in conditioning mode (27.5nF, 40 sparks), then conditioning	2	0.167	40+ 20	∼ 500	N	In the end, Eb too high to be measured: Vb>12kV, Eb>600MV/m
2	Contitioning	0.1	0.004	100	460 ± 120	N	
3	Contitioning	0.01	0.004	103	350 ± 50	N	

Table A.3: *Spark cycle mode* with β measurements for two molybdenum samples: sample Mo9 electropolished, and sample Mo11, electropolished and heat treated (UHV, 2 h, 1000 °C). Note that the large errors on the diametre arises from the way it is measured (cf. Fig. 4.1).

Spot no.	C_1 [nF]	C_2 [nF]	n_{tot}	D [µm]	HV probe	Comments
Sample Mo9 — Electropolished						
1	27.5	0.167	∼150	1000 ± 200	N	Unconditioned tip, not thightend properly, created double spot
2	27.5	0.167	40	900 ± 500	N	
3	27.5	0.167	40	800 ± 400	N	
4	27.5	0.167	(n?)	—	N	FAILED
5	27.5	0.167	20	600 ± 300	N	
6	27.5	0.167	10	600 ± 300	N	
7	27.5	0.167	10	600 ± 200	N	
8	27.5	0.167	5	500 ± 500	N	
9	27.5	0.167	5	380 ± 90	N	
10	27.5	0.167	1	300 ± 400	N	
11	27.5	0.167	1	300 ± 500	N	
Sample Mo11 — Electropolished and heat treated						
15	27.5	0.167	4	400 ± 400	N	300 β measurements
16	27.5	0.167	5	400 ± 300	N	
17	27.5	0.167	5	400 ± 200	N	
18	27.5	0.167	10	500 ± 300	N	
19	27.5	0.167	10	500 ± 200	N	
20	27.5	0.167	20	500 ± 100	N	
21	27.5	0.167	20	700 ± 200	N	
22	27.5	0.167	40	800 ± 300	N	
23	27.5	0.167	40	1000 ± 500	N	

Table A.4: Single sparks in *breakdown rate mode* on molybdenum, sample Mo6, standard milled and cleaned surface. The diametre was not measured since most of the spots were not possible to locate with the scanning electron microscope.

Spot no.	C_1 [nF]	C_2 [nF]	E_b [MV/m]	HV probe
18	0.1	0.004	FAILED	N
19	0.1	0.004	300	Y
20	0.1	0.004	300	N
21	0.1	0.004	400	N
22	0.1	0.004	400	Y
23	0.1	0.004	500	Y
24	0.1	0.004	500	N
25	27.5	0.167	FAILED	Y
26	27.5	0.167	300	Y
27	27.5	0.167	300	N
28	27.5	0.167	400	N
29	27.5	0.167	400	Y
30	27.5	0.167	400	Y
31	27.5	0.167	500	Y
32	27.5	0.167	500	N
35	2	0.167	300	Y
36	2	0.167	300	Y
37	2	0.167	500	Y
38	2	0.167	500	Y

Table A.5: Single sparks on molybdenum sample Mo11, electropolished and heat treated (UHV, 2 h, 1000 °C). Note that the large errors on the diametre arises from the way it is measured (cf. Fig. 4.1).

Spot no.	Measurement mode	C_1 [nF]	C_2 [nF]	E_b [MV/m]	D [µm]	HV probe
1	Conditioning	0.1	0.004	225	90 ± 80	N
2	Conditioning	0.1	0.004	197	—	N
3	Gap measurement	0.1	0.004	—	—	N
4	Breakdown rate	0.1	0.004	400	200 ± 200	N
5	Breakdown rate	0.1	0.004	400	500 ± 400	N
6	Breakdown rate	2	0.004	400	160 ± 120	N
7	Breakdown rate	2	0.004	400	160 ± 140	N
8	Conditioning	2	0.004	333	80 ± 10	N
9	Conditioning	2	0.004	342	80 ± 20	N
10	Conditioning	27.5	0.167	107	150 ± 110	N
11	Conditioning	27.5	0.167	245	160 ± 120	N
12	Breakdown rate	27.5	0.167	400	400 ± 400	N
13	Breakdown rate	27.5	0.167	400	300 ± 200	N
14	Field Emission	27.5	0.167	—	—	N

B Copper results

The data presented in this appendix makes the foundation for the Cu results and conclusions in this work.

Table B.1: Conditioning curves at different capacitances, sorted from the lowest to the highest. These spots are all from sample Cu 7, as described in Tab. A.1, the table continues onto the next page.

C_1 [nF]	Breakdown field	Field enhancement factor	Local breakdown field	Spot no.
0.01	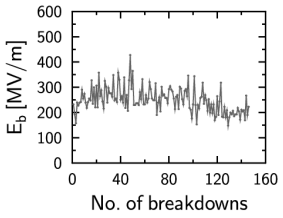	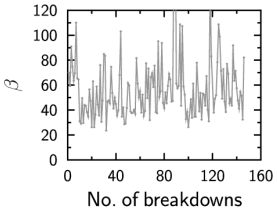	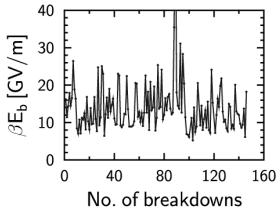	14
0.1	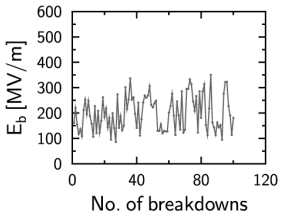	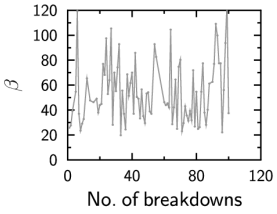	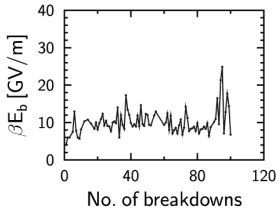	9
	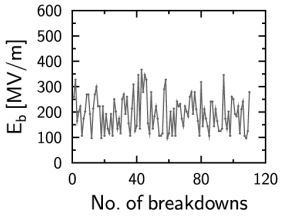	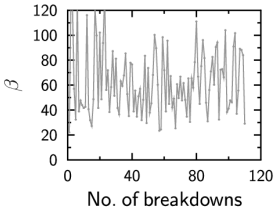	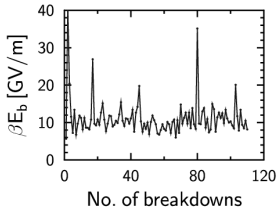	12
0.56	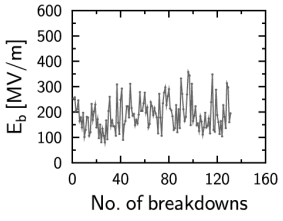	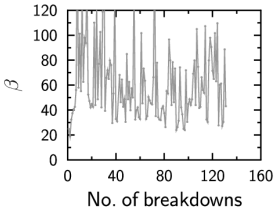	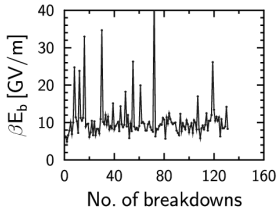	11

C_1 [nF]	Breakdown field	Field enhancement factor	Local breakdown field	Spot no.
0.56	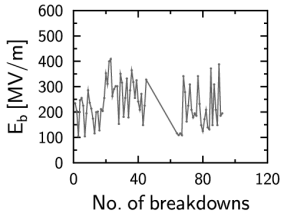	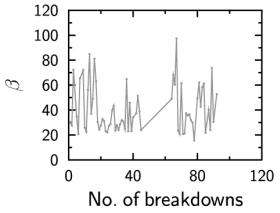	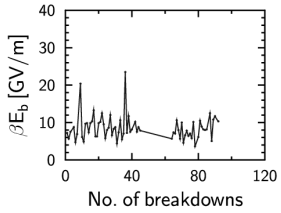	6
2	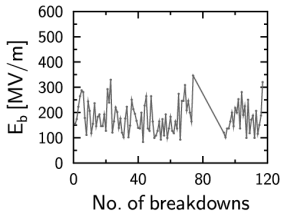	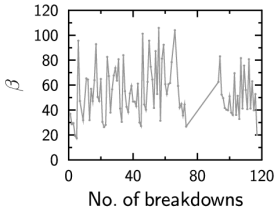	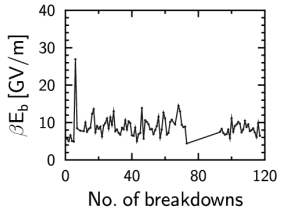	5
	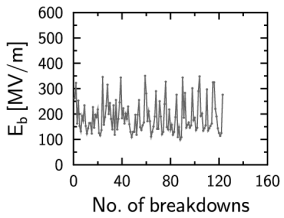	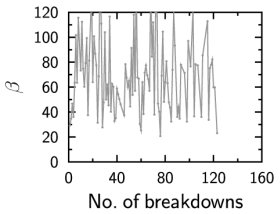	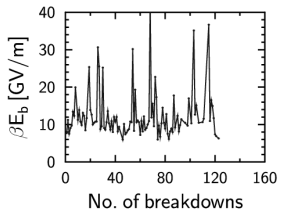	13
15	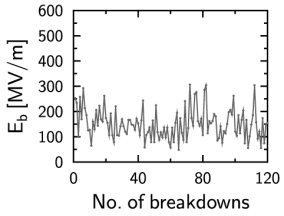	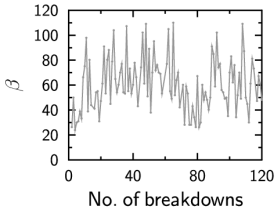	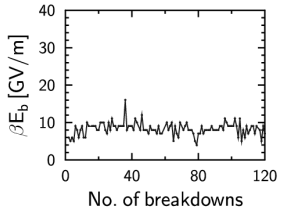	3
	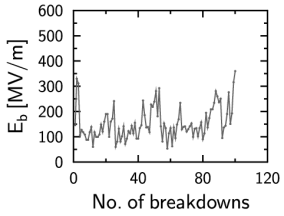	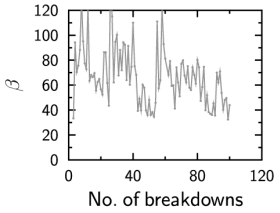	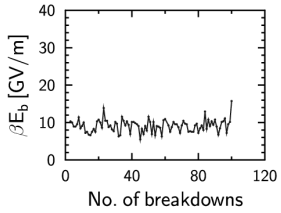	18
27.5	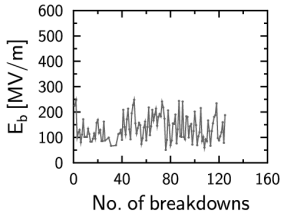	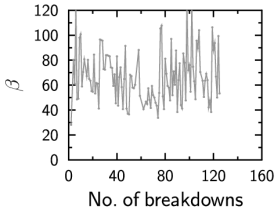	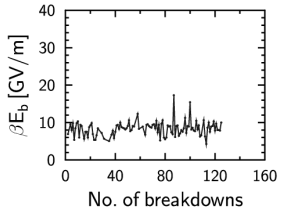	2
	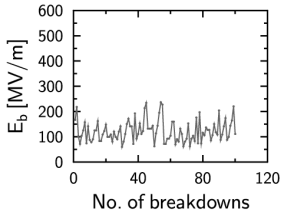	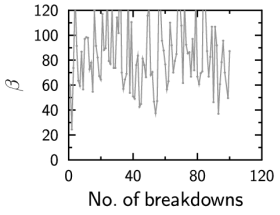	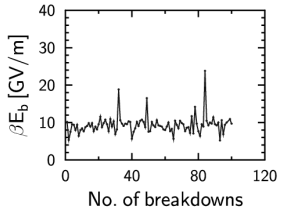	19

C Molybdenum results

The data presented in this appendix makes the foundation for the Mo results and conclusions in this work.

Table C.1: Conditioning curves at different capacitances, sorted from the lowest to the highest. The first two spots are from sample Mo10, whereas the rest are all from sample Mo 6, as described in Tab. A.2. The table continues for two more pages.

C_1 [nF]	Breakdown field	Field enhancement factor	Local breakdown field	Spot no.
0.01	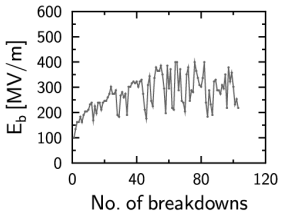	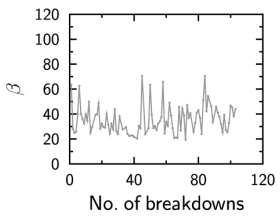	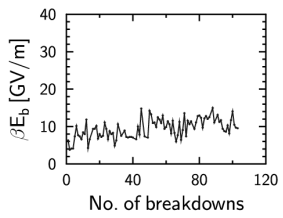	3
0.1	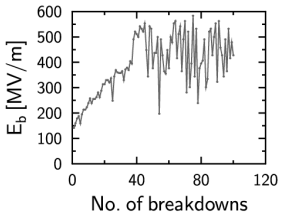	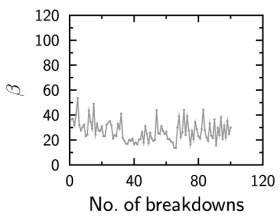	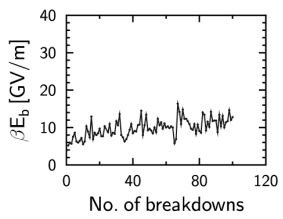	2
	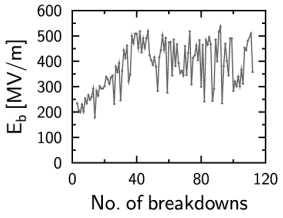	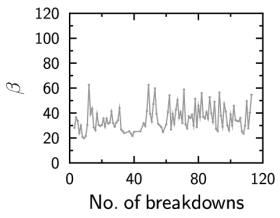	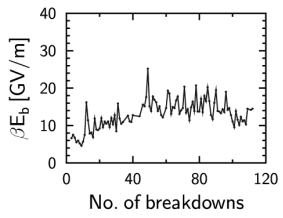	16

C_1 [nF]	Breakdown field	Field enhancement factor	Local breakdown field	Spot no.
0.56	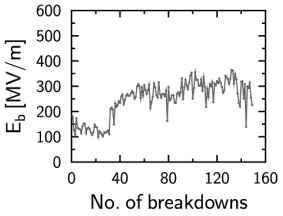	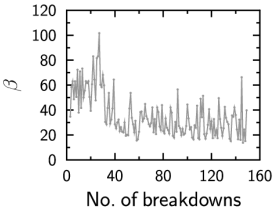	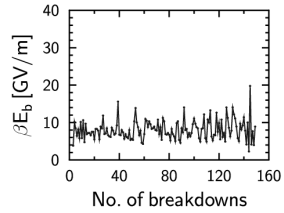	11
	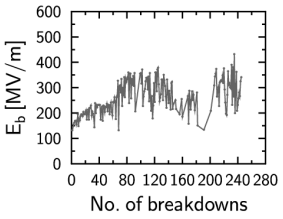	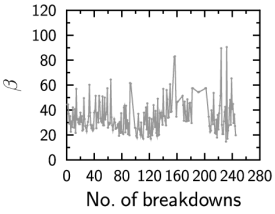	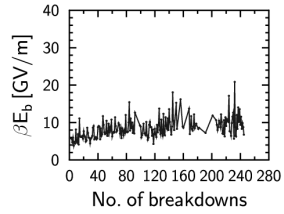	14
	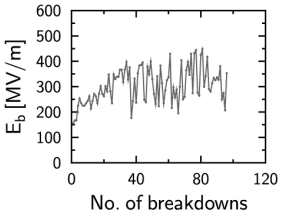	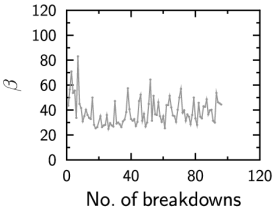	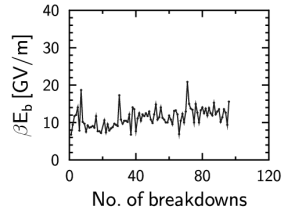	17
2	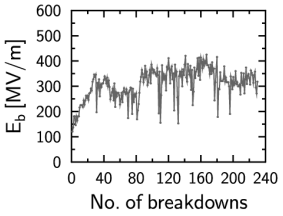	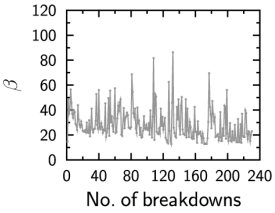	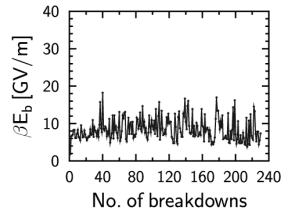	8
	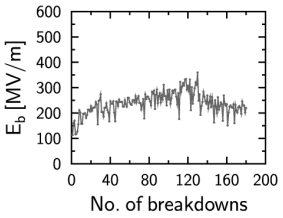	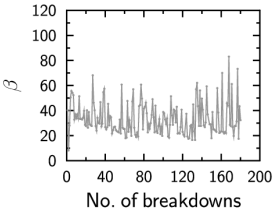	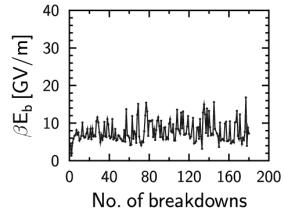	9
	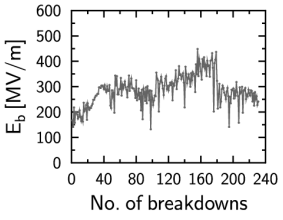	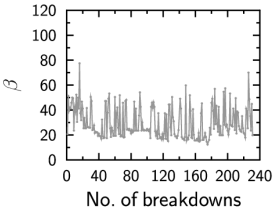	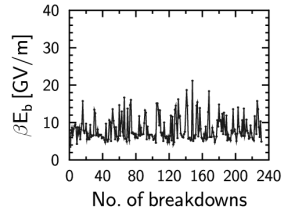	10

C_1 [nF]	Breakdown field	Field enhancement factor	Local breakdown field	Spot no.
15	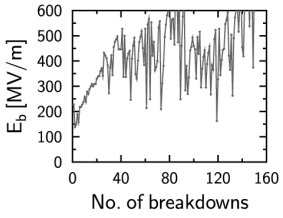	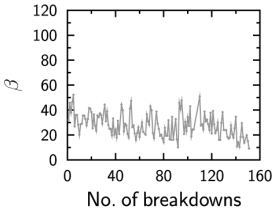	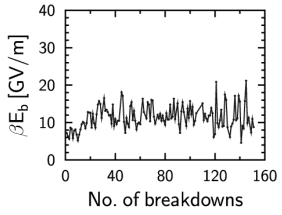	5
	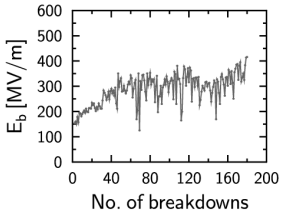	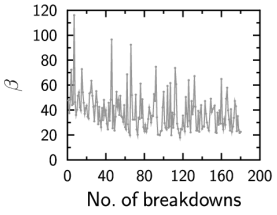	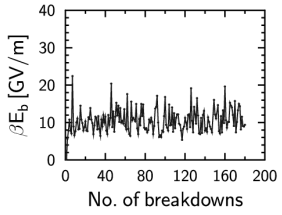	6
	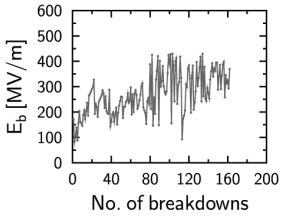	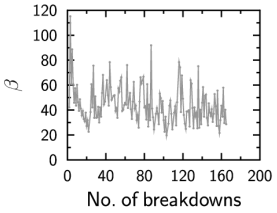	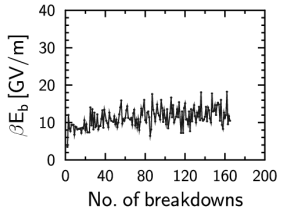	7
27.5	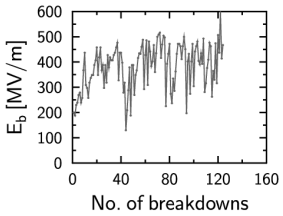	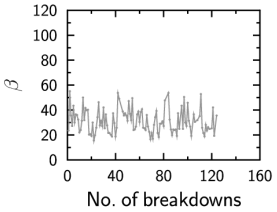	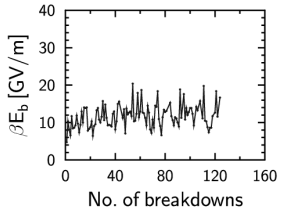	2
	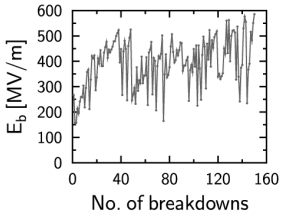	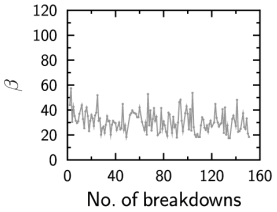	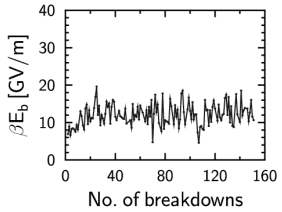	3
	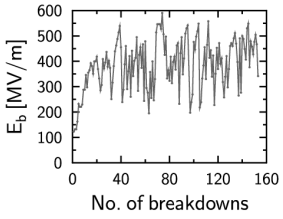	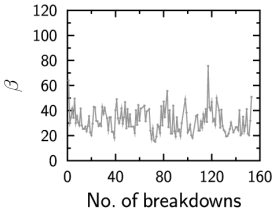	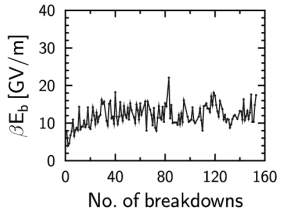	4

D Comparing Cu and Mo

The plots presented here are a combination of those already presented in Fig. 4.2, and 4.7, 4.9, and 4.10, it is only repeated to give a better overview and to ease the comparison of the two materials tested in this work.

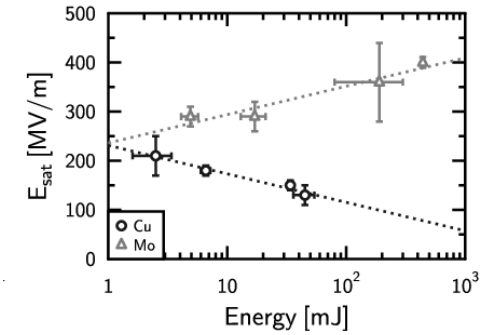

(a) Saturated field

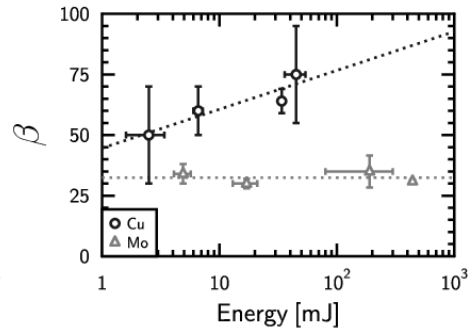

(b) Average field enhancement factor

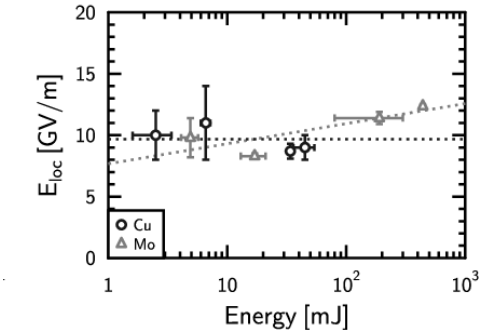

(c) Average local field

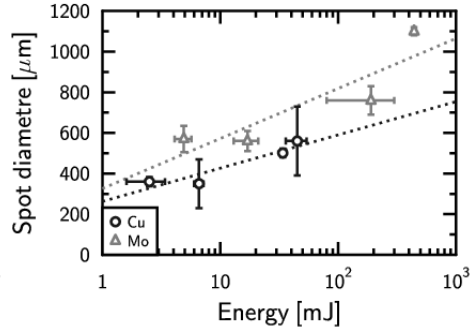

(d) Spot diametre

Figure D.1: Four of the different breakdown parameters studied in this work, all displayed as a function of energy.